Hypertrophic Cardiomyopathy

16

Raymond H.M. Chan and Martin S. Maron

Hypertrophic cardiomyopathy (HCM) is a common genetic cardiomyopathy caused by mutations in genes which encode for the myofilament protein components of the sarcomere or the z-disc [1–4]. It has a prevalence of 1 in 500 in the general population and is a global disease affecting patients in all continents [5] and of both genders [6]. It is the leading cause of sudden death in young people, with an annual mortality rate of 1 % [7]. Since its first description over 50 years ago, the pathophysiology of the disease is still incompletely understood [8]. The disease is associated with tremendous heterogeneity with regard to its presentation, phenotype, and prognosis. The diagnosis for HCM is usually made clinically after symptom onset or cardiac events, but may also be found after routine 12-lead electrocardiogram (ECG), heart murmur on cardiac exam, or in family screening of probands.

R.H.M. Chan, MD, MPH, FRCP(C), BScPhm (✉)
Division of Cardiology,
Beth Israel Deaconess Medical Center,
PERFUSE Study Group, 330 Brookline Avenue,
East Campus SH 462, Boston, MA 02215, USA
e-mail: rhchan@bidmc.harvard.edu

M.S. Maron, MD
Cardiac CT and MRI, Division of Cardiology,
Hypertrophic Cardiomyopathy Center,
Tufts University School of Medicine,
Tufts Medical Center, 800 Washington St, #70,
Boston, MA 02111, USA
e-mail: mmaron@tuftsmedicalcenter.org

Imaging

Clinical diagnosis is confirmed through imaging using 2D echocardiography and/or cardiac MRI (CMR) or CT by identifying an increase in left ventricular (LV) wall thickness ≥15 mm (mean ~22 mm [normal ≤12 mm]) without a dilated LV chamber in absence of other cardiac or systemic disease processes (e.g., aortic stenosis, chronic hypertension) capable of producing the magnitude of hypertrophy [9]. In certain instances, such as patients with a family history of HCM, a maximal wall thickness ≥13 mm may be compatible with the diagnosis of HCM. LV hypertrophy is most commonly asymmetric, with the most common location of increased wall thickness occurring in the contiguous area of the basal anterior septum and anterior wall [10] (Fig. 16.1), although there is tremendous heterogeneity in phenotypic expression, even in those with a common genotype. In addition, in close to 25 % of HCM patients, segments of LV hypertrophy can be separated by myocardial regions of normal thickness, i.e., noncontiguous pattern of LV hypertrophy. Concentric pattern of LV hypertrophy occurs very rarely in HCM (~1 %) [11, 12] (Fig. 16.2).

Characterization of Anatomy

LV Hypertrophy

CMR has the unique ability to acquire truly tomographic high-resolution images in any anatomic

F. Saremi (ed.), *Cardiac CT and MR for Adult Congenital Heart Disease*,
DOI 10.1007/978-1-4614-8875-0_16, © Springer Science+Business Media New York 2014

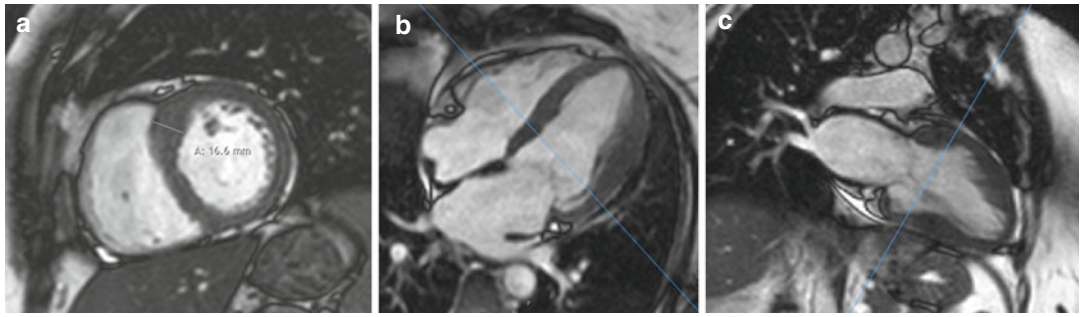

Fig. 16.1 Focal myocardial hypertrophy. Images in different planes (with corresponding scanlines) serve as a reference "road map" to pinpoint the location of focal hypertrophy and to precisely measure the true maximal wall thickness, a metric which has been associated with increased risk of cardiac events. (**a**) In this HCM patient, a basal short-axis slice shows a focal area of increased septal wall thickness confined to the anterior septum with normal wall thickness in other segments. Maximal wall thickness was 16.6 mm. Corresponding 4-chamber (**b**) and 2-chamber (**c**) views demonstrate the difficulty in appreciating the true geometry of the left ventricle walls without the short-axis slice

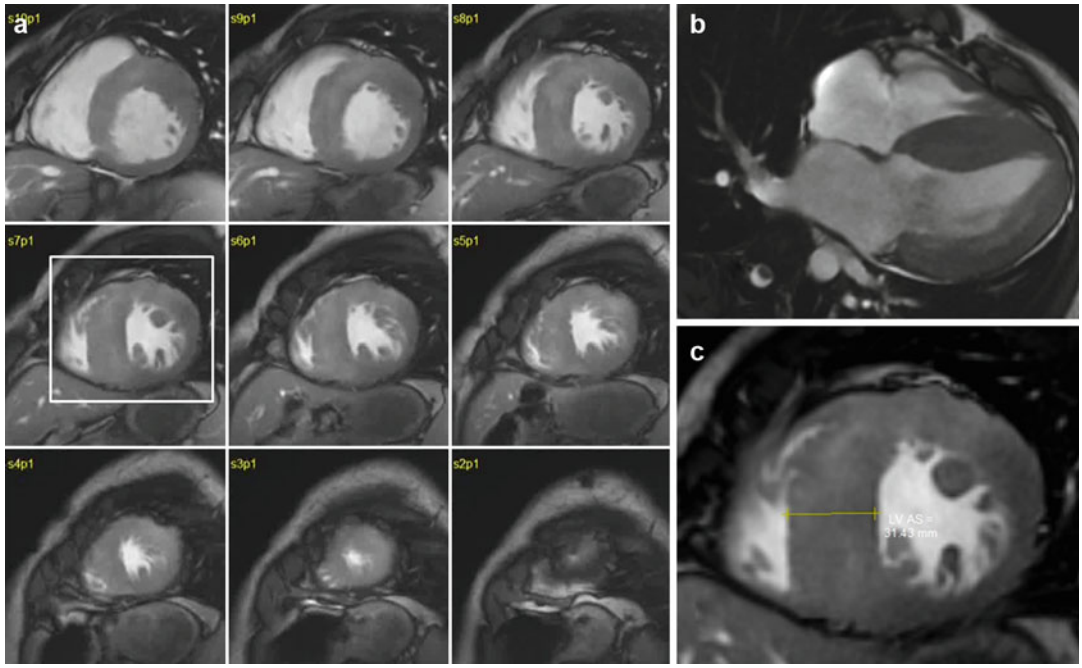

Fig. 16.2 Concentric hypertrophy on the left ventricle (LV). (**a**) Short-axis stack shows extreme hypertrophy in most segments. Note the relative sparing of the right ventricular walls. (**b**) 4-chamber slice showing the degree of hypertrophy in all of the LV walls. (**c**) Enlarged view of slice 7, showing maximal wall thickness of 31 mm. Overall LV mass was 311 g, with an LV mass index of 185 g/m^2. Based on this finding and after a balanced discussion with the patient, a prophylactic ICD was placed due to the high risk of sudden death associated with extreme hypertrophy

plane without ionizing radiation, thus making it a particularly useful tool for precisely characterizing the HCM phenotype. Balanced steady state free precession (SSFP) cine imaging sequences result in a sharp delineation of myocardial borders due to the high contrast between a relatively dark myocardium and bright blood pool. This allows for accurate measurements of wall thickness in any region of the LV chamber. By using contiguous short-axis slices, a clear and comprehensive presentation of the entire myocardial geometry from the base to apex can be achieved, resulting in precise and reproducible quantification of chamber volumes, LV mass, and systolic function (Figs. 16.1 and 16.2).

Focal areas of LV hypertrophy in the anterolateral free wall, apex, and posterior septum may not be well seen (or the extent underestimated) by echocardiography due to the inability to discriminate the epicardial borders of the heart from noncardiac structures, or due to anatomic interference from thoracic or pulmonary parenchyma (Fig. 16.3). Furthermore, there is evidence to suggest that in some HCM patients, echocardiography can substantially underestimate the magnitude of hypertrophy compared with CMR [13], particularly in patients with focal areas of increased LV wall thickness confined to the anterolateral wall [14] (Fig. 16.3c).

Apical HCM is characterized by hypertrophy of the myocardium, predominantly in the left ventricular apical area. This variant of HCM is rare in Western countries (1–2 %) but is common in Japanese and other Asian populations (up to 25 %). Typical features of apical HCM include giant negative T waves on ECG, mild symptoms, and a generally more benign course. Other morphological findings of this disease include cavity obliteration and apical sequestration (Fig. 16.3). Echocardiography has limitations for demonstration of the apex and may miss apical HCM. This limitation is not encountered with cardiac MRI.

CMR can also easily facilitate the identification of patients with massive hypertrophy (maximal wall thickness ≥30 mm) which is considered a high-risk feature and warrants consideration of primary prevention implantable cardioverter-defibrillator (ICD), even in the absence of any other risk markers (Fig. 16.2) [15]. CMR can identify myocardial crypts, which are more common in genotype-positive but phenotype-negative patients (i.e., without LV hypertrophy), and may help identify HCM family members to be considered for diagnostic genetic testing (Fig. 16.4) [16, 17].

LV mass calculated from planimetry of short-axis slices provides an excellent assessment of the overall extent of LV hypertrophy, as there is tremendous variability in the patterns of hypertrophy in regions remote from maximal LV wall thickness. LV mass is therefore a more robust measure of the overall extent of LV hypertrophy. There is recent evidence that marked increase in LV mass index may be more sensitive in predicting adverse outcome (including sudden death), while maximal wall thickness >30 mm was more specific [18]. However, its relevance as an independent marker for predicting adverse outcomes such as sudden death (SD) is still not well defined.

RV Hypertrophy

Precise delineation of right ventricular morphology has been challenging with echocardiography due to its complex three-dimensional geometry and its orientation within the thorax. The unique ability of CMR or CT to obtain or reconstruct images in any orientation provides tools for robust assessment of the RV. Recent studies have demonstrated increased RV wall thickness (≥8 mm) in over 1/3 of HCM patients, with an important proportion of patients who have an increased RV wall mass [19, 20].

In addition, approximately half of HCM patients will demonstrate hypertrophy of the septal band and the crista supraventricularis (Fig. 16.5) which is an RV muscle structure that is often positioned adjacent to the basal anterior septum [21–23]. As a result, it can sometimes be erroneously included in the measurement of the ventricular septum, which can lead to overestimations in LV maximal wall thickness. It is important to clarify the anatomy by carefully examining cine loops and seeing the crista move off the septum at various stages of the cardiac cycle. The morphological phenomena of hypertrophied crista supraventricularis and increased RV wall thickness support the principle that HCM is a disease process that can involve the right ventricle, rather than exclusively the LV.

LV Outflow Tract Obstruction

Subaortic obstruction in HCM is caused by anterior leaflet of the mitral valve (rarely the posterior leaflet) making contact with basal septum in mid-systole (SAM-septal contact) (Figs. 16.6 and 16.7). The Venturi effect was originally hypothesized to be the mechanism by which systolic anterior motion (SAM) of the mitral valve leaflet and chordal structures occurs. However, recent evidence has pointed to flow drag, which is the

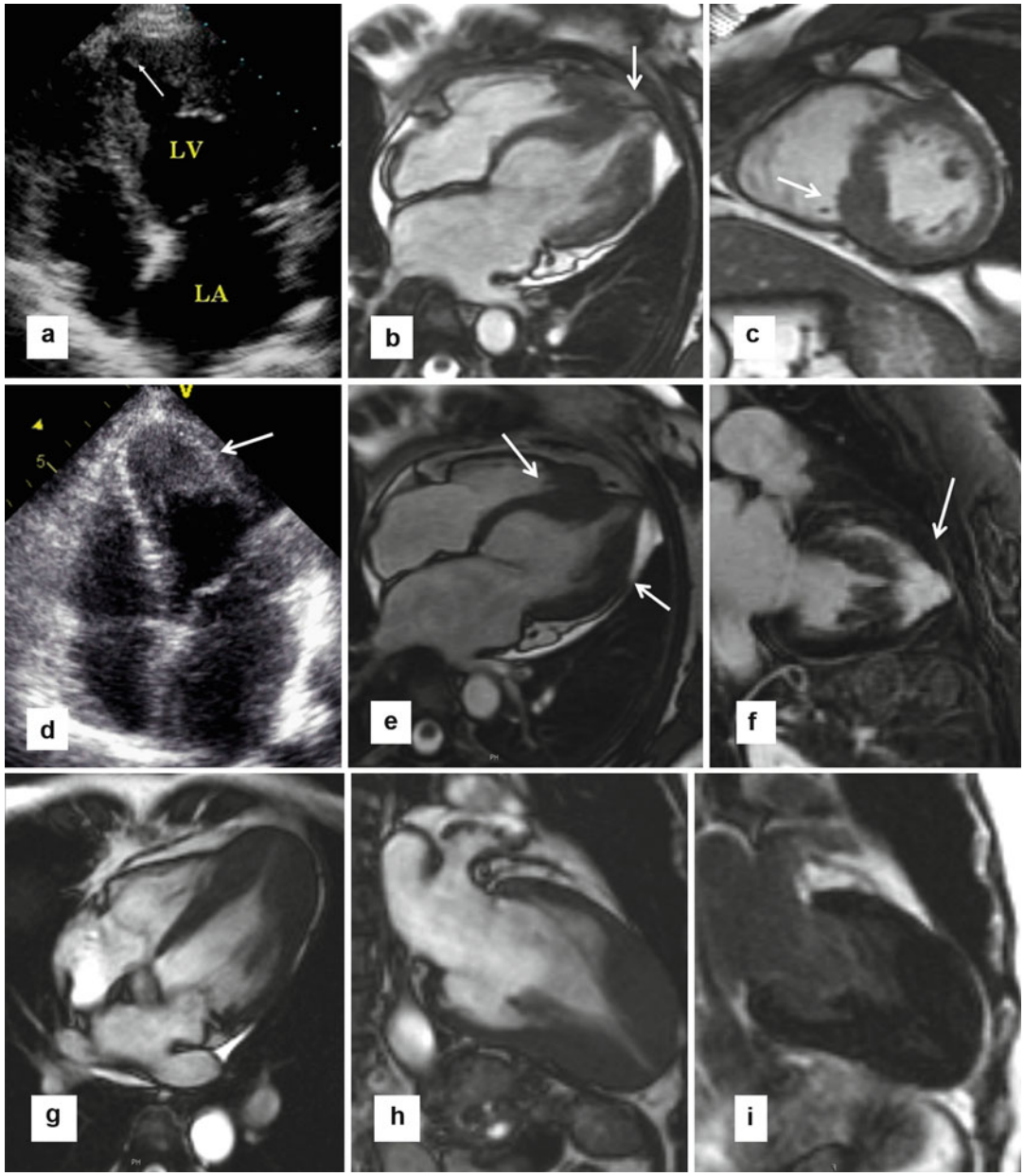

Fig. 16.3 Echocardiography weaknesses. (**a**, **b**) Patient with flipped T waves on lateral leads during a screening ECG leads to echocardiography, but was nondiagnostic due to incomplete visualization of the apex and apical lateral walls (**a**). In this case, steady state free precession (SSFP) MR (**b**) showed substantial hypertrophy at the apex as well as a small apical aneurysm (*arrow*). (**c**) Focal hypertrophy of the mid-inferior septum (*arrow*), which was underappreciated in echocardiography. (**e**, **f**) In a different patient, echocardiography suggested thickening of the apex (*arrow* in **d**); however, the endocardial borders were not clearly visualized. Corresponding 4-chamber cine slice (**e**) precisely delineating the degree and location of apical hypertrophy (*arrows*). Late gadolinium enhancement (LGE) imaging shows extensive enhancement in the apex and the anterior wall (*arrow*). (**g**–**i**) Patient with apical variant HCM without evidence of LGE. 4-chamber (**g**) and 2-chamber SSFP images clearly show the hypertrophy localized to the apex. 2-chamber late gadolinium enhancement (**i**) shows no abnormal enhancement

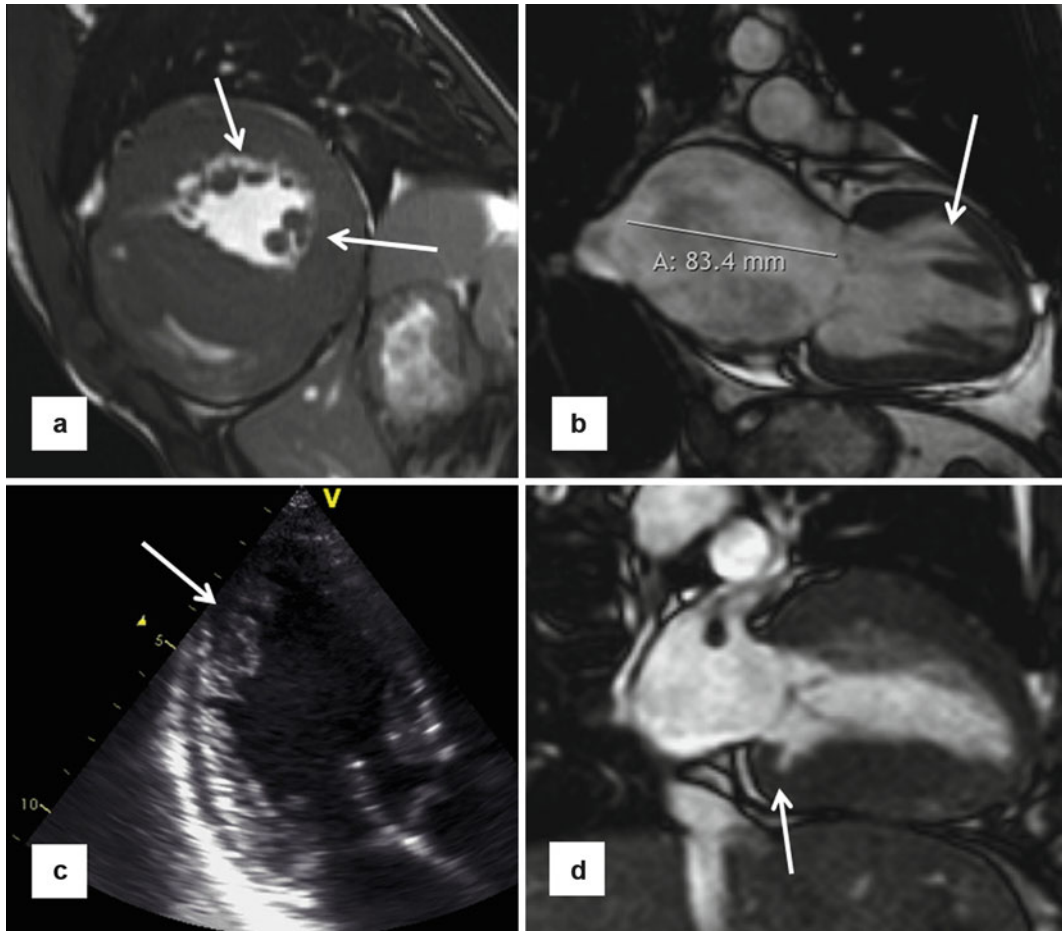

Fig. 16.4 Different phenotypic expressions of HCM. (**a**) Multiple accessory papillary muscles (*arrows*) seen on short-axis CMR. (**b**) End-stage HCM with left ventricle ejection fraction =30 %. Note the markedly enlarged left atrium and the presence of apicobasal bundle (*arrow*). (**c**) Myocardial crypts (*arrow*) seen in mid-inferolateral wall on echocardiogram in 3-chamber view. (**d**) Different patient with a myocardial crypt (*arrow*) seen in basal inferior wall

force of flow from a hyperdynamic ventricle, to be the primary hemodynamic force for pushing the mitral valve toward the septum. Hence, complete characterization of the mitral valve apparatus (including the chordal structures and papillary muscles), and their influence on the pathophysiology of LV outflow tract (LVOT) obstruction, has important therapeutic implications. There is also emerging evidence that the angle between LVOT and aortic root may be related with outflow tract gradient [24]. The elevated LV systolic pressures resulting from outflow tract obstruction lead to increased wall stress, venous congestion, myocardial ischemia, and mitral regurgitation. Fibrosis may lead to diastolic dysfunction and may also be a substrate for unstable arrhythmias (see discussion below on LGE).

Cine CMR can accurately locate in 3 dimensions the origin of high-velocity blood flow, frequently in the region of SAM-septal contact, which is visualized as a signal void from dephased blood (Fig. 16.6). Although SSFP sequences are less sensitive to dephasing from turbulent blood flow compared with gradient recalled echo (GRE) sequences, hemodynamically significant outflow tract gradients usually result in visually apparent signal voids to easily locate the origin of the obstruction. Phase contrast (PC) MR can

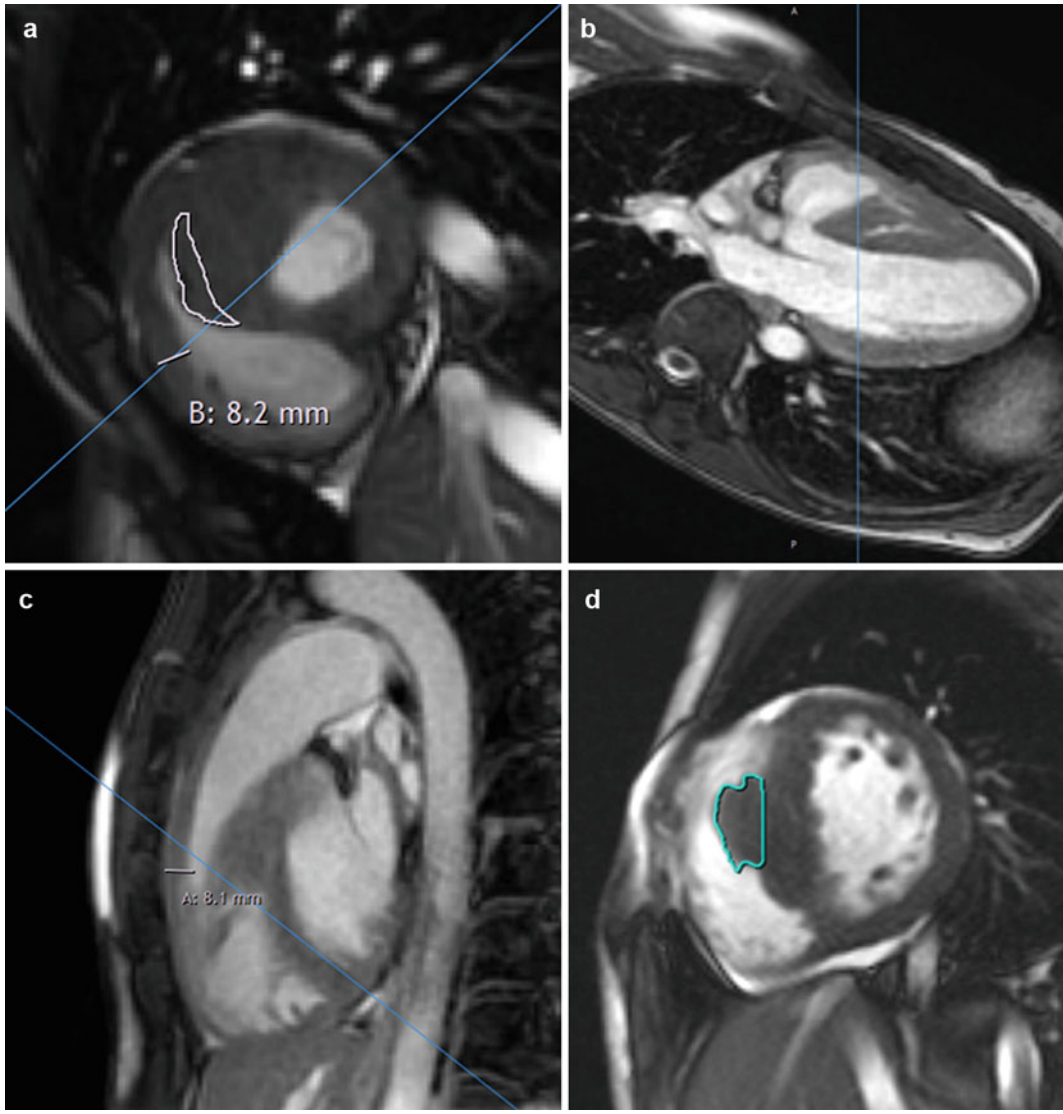

Fig. 16.5 Right ventricular (RV) septomarginal trabeculation and crista supraventricularis can be mistakenly incorporated in the intraventricular septum measurements. (**a**) HCM patient with very prominent septal band muscle (*outlined in white*), as well as increased thickness of right ventricular anterior free wall of 8.2 mm. Due to the location of this muscle adjacent to the septum, incorrect inclusion of its dimensions when measuring the left ventricle (LV) septal thickness may lead to overestimation of the maximum LV wall thickness. Close inspection of the cine short-axis stack confirms that this structure indeed moves away from the septum toward the RV cavity. Furthermore, views from other orientations with scanlines in (**b**) (modified 5-chamber view) and (**c**) (RV outflow tract view) confirm the location of the circumscribed area of thickness is in the right ventricular cavity rather than part of the septum. (**d**) Another patient with hypertrophied septomarginal trabeculation, with its structure outlined

be obtained if subaortic hypertrophic obstructive cardiomyopathy (HOCM) is suspected. For accurate measurements, it is important that the plane of PC image is adjusted perpendicular to jet of blood flow in subaortic region and the velocity encoding (VENC) value is set high enough to prevent aliasing. However, due to the superior temporal resolution of Doppler echocardiography,

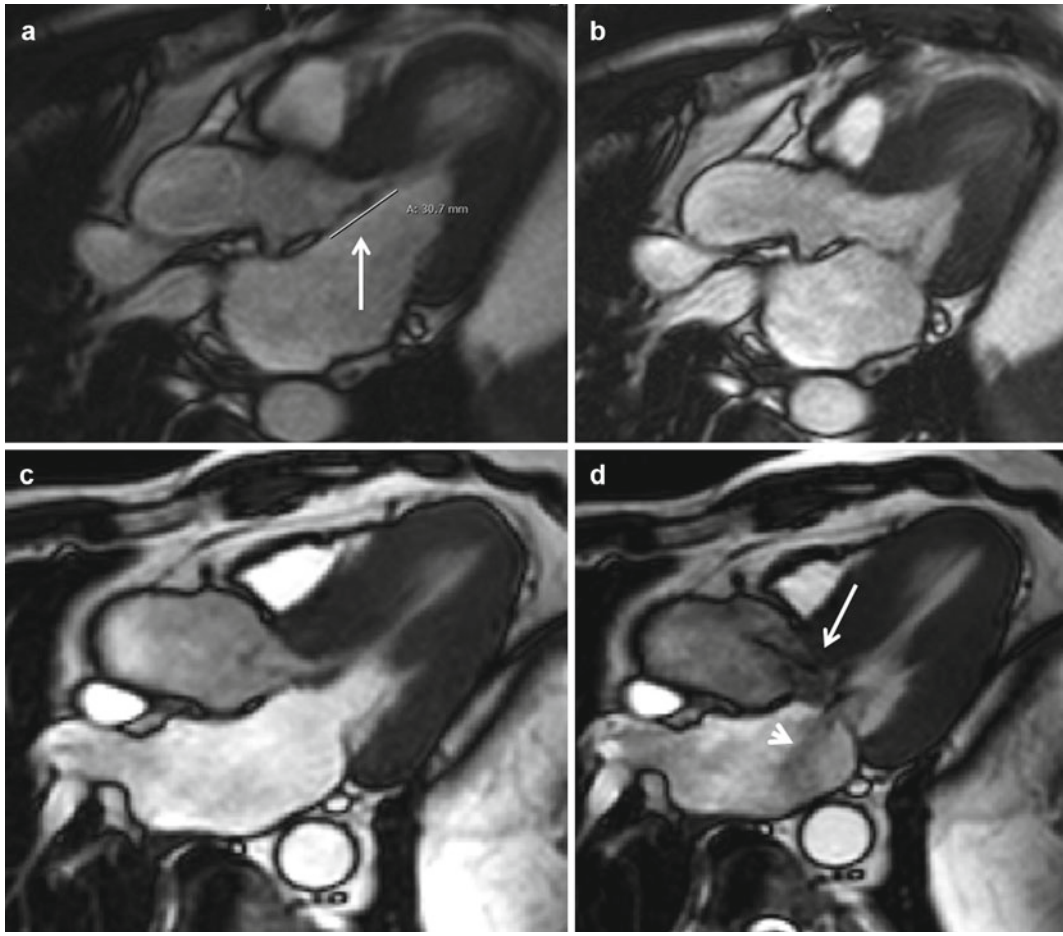

Fig. 16.6 Elongation of mitral valve leaflet length has been identified as a primary phenotypic abnormality in patients with HCM phenotype or genotype. (**a**) Patient with anterior mitral leaflet length of 31 mm (*arrow*), (**b**) Without systolic anterior motion or mitral regurgitation. (**c**) Patient with anterior mitral leaflet length of 31 mm and posterior mitral leaflet length of 23. (**d**) There was marked leaflet and chordal systolic anterior motion leading to an LVOT gradient of >80 mmHg. Note the dephasing jet indicative of turbulence through the LVOT (*arrow*) as well as dephased blood in left atrium (*arrowhead*) indicative of mitral regurgitation

it is preferable to use gradient measurements obtained from echocardiography when making treatment decisions.

Furthermore, fixed LVOT obstruction by a subvalvular membrane and aortic valve stenosis must be ruled out, usually through the use of echocardiography. The presence of an outflow tract gradient in the absence of SAM-septal contact is highly suggestive of a subaortic membrane.

Basal LVOT gradients ≥30 mmHg due to SAM-septal contact are a strong independent determinant of heart failure (HF) symptom progression, HF death, stroke death, and all-cause mortality [25]. The identification of obstruction at rest or following exercise opens up treatment options not available to nonobstructed patients, including surgery and alcohol septal ablation. Therefore, identifying obstruction is a critical issue in the diagnostic workup for HCM patients.

The limiting factor is the dynamic nature of LVOT obstruction [26, 27], where CMR can only assess a patient reliably under basal conditions. One-third of HCM patients will only have outflow obstruction transient during activity or provocation. Thus, clinical management decisions regarding

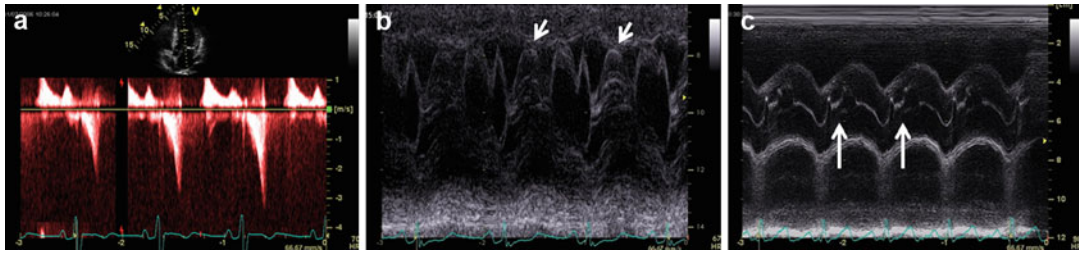

Fig. 16.7 Some classical echocardiographic findings found in HCM patients with left ventricle (LV) outflow tract obstruction, illustrating the anatomy and hemodynamic effects as a result of the obstruction. (**a**) Continuous wave Doppler through the LV outflow tract in 5-chamber view showing typical dagger-shaped flow indicative of dynamic obstruction. (**b**) M-mode through mitral valve leaflets in parasternal long axis showing valvular systolic anterior motion (*arrows*). (**c**) M-mode through aortic valve leaflets in parasternal long axis showing premature closure in mid-systole (*arrows*)

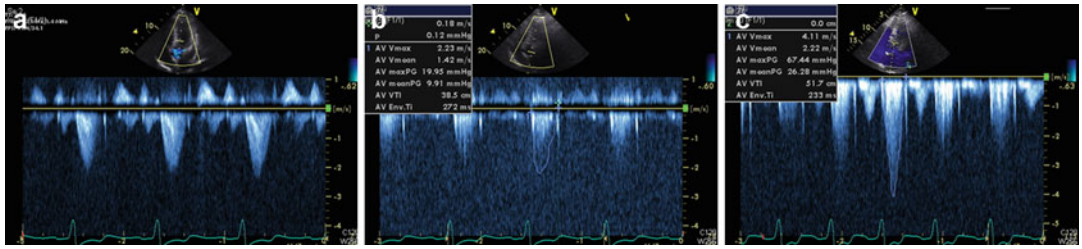

Fig. 16.8 Left ventricle (LV) outflow tract obstruction is a dynamic process. This is an echocardiogram of an HCM patient with marked dyspnea during exertion showing continuous wave Doppler gradients across LV outflow tract. (**a**) At rest – no significant gradient seen. (**b**) With Valsalva maneuver – no significant change in gradients. (**c**) During exercise – significant LV outflow tract obstruction with peak gradient >60 mmHg. Patient's symptoms were well controlled with titrating doses of beta-blockers

outflow obstruction should be predicated on measurements from echocardiography (with or without stress/provocative maneuvers) (Fig. 16.8) [28].

Papillary Muscles

Abnormalities in papillary muscle morphology are common, including papillary muscle hypertrophy, anteroapical displacement, double bifid, direct insertion into mitral leaflets, fusion to ventricular septum or free wall [11, 29–32], and accessory papillary muscles (including apicobasal muscle bundles [33]) (Fig. 16.9). Cardiac MR can be used to reliably characterize papillary muscle anatomy by accurately identifying their number, location, and position in the LV chamber (Fig. 16.10). When compared with controls, there appears to be an increased number of papillary muscles, in addition to an increased papillary muscle mass. Papillary muscle mass is related to overall LV mass index. However, subgroups of patients have normal LV mass but increased papillary muscle mass [30]. These observations broaden our understanding of HCM phenotype to include structures beyond the left ventricular wall and suggest that the same disease pathophysiology responsible for LV hypertrophy may also be involved in papillary muscle hypertrophy.

Certain abnormalities in papillary muscle anatomy have been shown to be related to LVOT obstruction. Papillary muscles appear to be positioned more anteriorly and closer to the ventricular septum in those with LVOT obstruction at rest and had more marked hypertrophy compared to those without obstruction [30]. Anteroapical displacement of anterolateral papillary muscles and double bifid papillary muscles have been found to be independently associated with significant outflow gradients, even after controlling for septal thickness [29]. Patients with significant outflow tract obstruction also have papillary muscles

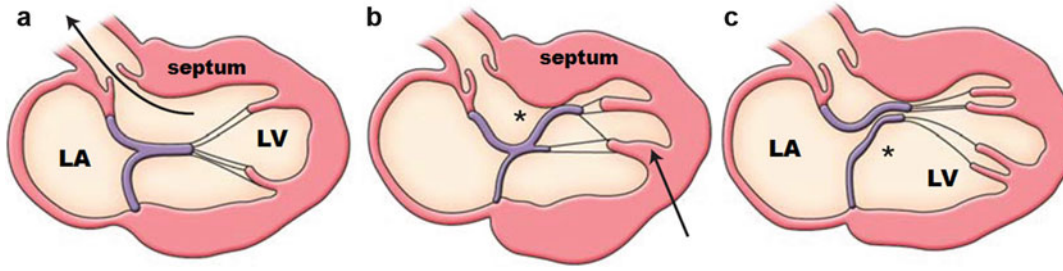

Fig. 16.9 Schematic of septum, papillary muscle, and mitral valve anatomy and their contribution to LV outflow tract obstruction and mitral regurgitation. (**a**) Normal papillary muscle and mitral valve location and length. Note the unimpeded flow through the LV outflow tract. (**b**) Anteroapical displacement of thickened papillary muscle (*arrow*), with lengthened anterior mitral valve leaflet (*) and thickened septum leading to significant outflow tract obstruction. (**c**) Double bifid papillary muscles with lengthened posterior mitral valve leaflet (*), leading to chordal and valvular systolic anterior motion, outflow tract obstruction, malcoaptation, and mitral regurgitation (Figures copyright Raymond H Chan)

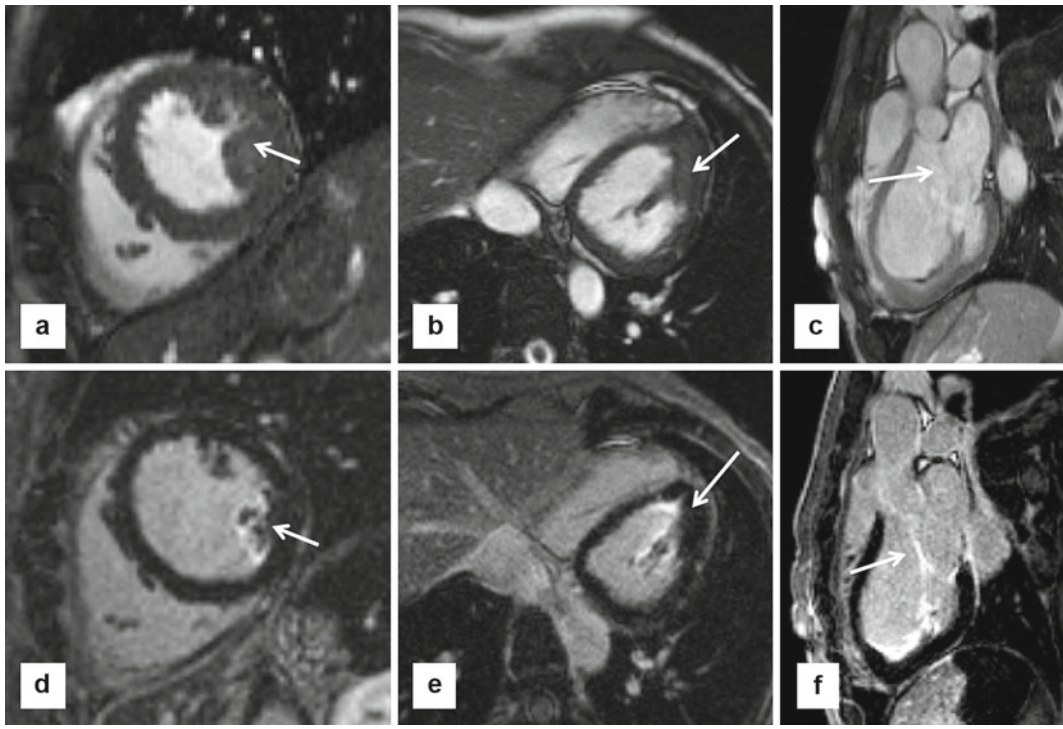

Fig. 16.10 Papillary muscle hypertrophy and mitral valve abnormalities are primary anatomic features of HCM, which affect more than the left ventricle (LV) walls. (**a**) Short-axis steady state free precession (SSFP) shows prominent size of posterior papillary muscle (*arrow*), despite relatively normal wall thicknesses. (**b**) Modified 4-chamber SSFP confirms marked enlargement of posterior papillary muscle (*arrow*). (**c**) LV outflow tract (LVOT) view shows elongated anterior mitral valve leaflet. (**d**–**f**) Show late gadolinium enhancement (LGE) imaging in corresponding views. Note enhancement seen in papillary muscle (**d**, **e**) and mitral valve leaflets (**f**) (*arrows*). The clinical significance of LGE in these structures is unknown

closer to the ventricular septum (Fig. 16.9) [30]. Prior to more widespread use of CMR, such abnormalities are often not well appreciated by echocardiography and thus missed and were only seen during surgery by direct inspection [22]. Papillary muscle mobility may also play an

important role in dynamic LV outflow tract obstruction during exercise (Fig. 16.8). Complete visualization of papillary muscle anatomy is therefore a clinically important step in the management of patients with LVOT obstruction.

The above evidence supports the hypothesis that accessory and apically displaced papillary muscles contribute significantly to LVOT obstruction, by pulling the plane of the mitral valve toward the septum. As a result, they are often removed during surgery, and therefore, their identification by imaging can aid in preoperative surgical planning. Furthermore, CMR can identify anomalous papillary muscle insertion into the mitral valve, which can redirect patients toward surgery rather than alcohol septal ablation, since this abnormality causes mid-ventricular obstruction not amenable to percutaneous approach.

Mitral Valve Leaflet Anatomy

Mitral valve leaflets appear to be elongated independently of other morphological characteristics such as LV thickness or mass and may represent a primary phenotypic characteristic of HCM [34]. Such elongated leaflets play an important role in generating LV outflow tract gradients, particularly in those whose relative anterior mitral leaflet length exceeds twice that of the transverse LV outflow tract diameter (Fig. 16.6) [34]. The anterior mitral leaflet (AML) has more redundancy and mobility [35]. There is also a significant relationship between the ratio of AML length and LVOT diameter with length and the magnitude of outflow tract gradient. Extreme lengths of the AML may potentially produce mitral-septal obstruction even after extensive septal muscle resection. Increased mitral valve leaflet length may also serve as a marker of gene-positive status in HCM in family members without LV hypertrophy.

As a result of mitral leaflet malcoaptation due to systolic anterior motion (SAM), mitral regurgitation jets can also be seen as a signal void in the left atrium. These jets are often posteriorly directed due to relatively greater SAM of the AML compared to the posterior leaflet (Fig. 16.6). The regurgitant jet volume can be quantitated by comparing the left ventricular stroke volume by planimetry of SSFP images with the aorta flow obtained from phase contrast sequences.

Planning for Surgical Myectomy

Surgical myectomy is the gold standard for symptomatic relief in patients with significant LV outflow obstruction on maximal medical therapy [9]. As outlined above, CMR can be helpful by clear delineation of the relative three-dimensional anatomy of the LV outflow tract, mitral valve, and the subvalvular apparatus [28]. Accessory papillary muscles which may contribute to obstruction can be identified for planned removal. Important measurements for operative planning include maximal septal thickness, distance of maximum thickness from aortic annulus, and the apical extent of septal bulge. Careful CMR planning using multiple thin slabs with no gaps in the LV outflow tract orientation can be extremely helpful by providing precise and reproducible measurements. This anatomic information should supplement rather than supplant those obtained from transesophageal echocardiogram (TEE).

Evaluation After Alcohol Septal Ablation

Using late gadolinium enhancement imaging, CMR can objectively quantify the amount of necrosed tissue, as well as its location in relationship to the LVOT (Fig. 16.11). This may help in the assessment of patients who achieve suboptimal results after ablation or when gradients recur late after the procedure.

LV Apical Aneurysms

HCM patients with LV apical aneurysms are a previously under-recognized subgroup prior to more widespread use of CMR in these patients. Its prevalence is low at 2 % [36]. It is characterized by thin-walled, akinetic, or dyskinetic segments in the LV apex (Fig. 16.12). Often, these segments are

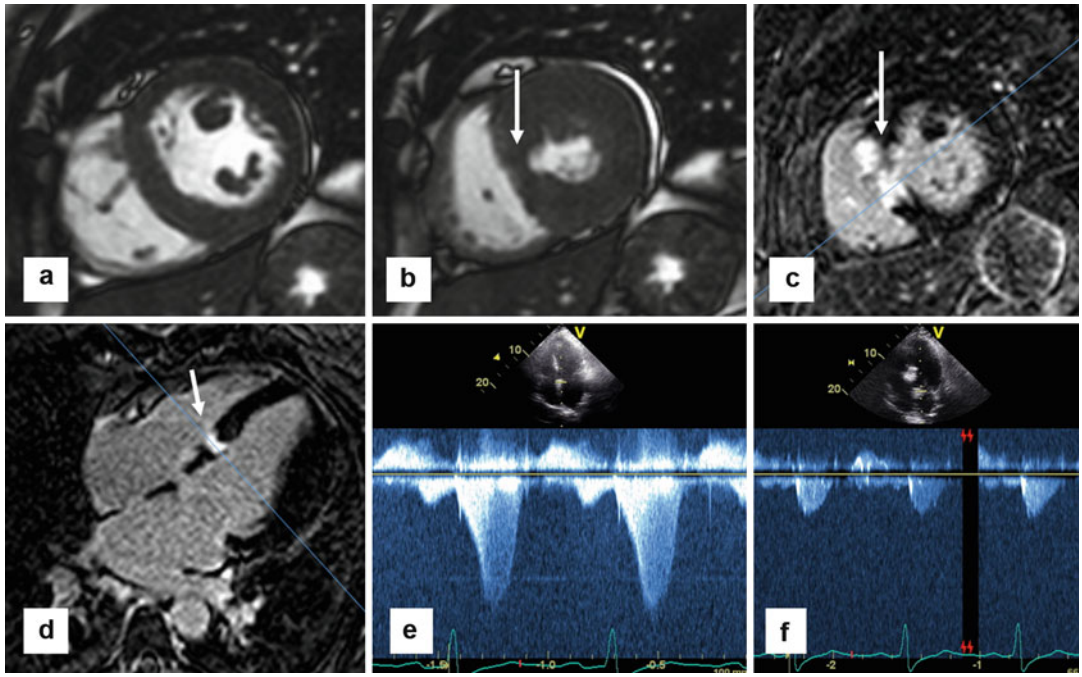

Fig. 16.11 Cardiac MR can be helpful in the evaluation of patients after alcohol septal ablation. These series of images are from a patient who had a successful alcohol septal 2 months prior to MR. (**a**) Short-axis steady state free precession (SSFP) slice showing small area of infarcted myocardium that fails to thicken during systole in (**b**) (*arrow*). Corresponding LGE imaging in short-axis (**c**) and 4-chamber view (**d**) showing focal area in the basal septum with bright transmural enhancement secondary to induced infarction from the alcohol septal ablation (*arrow*). (**e**) Prior to the alcohol septal ablation, continuous wave Doppler echocardiography shows a significant LVOT gradient well over 50 mmHg. (**f**) 2-month post-alcohol septal ablation, there is no clinically significant LVOT gradient

composed of fibrotic tissue which can be seen as a transmural pattern of late gadolinium enhancement (Fig. 16.13). Like apical hypertrophy, echocardiography may not reliably detect these aneurysms because of its technical limitations, where in one study the sensitivity was only 57 % [37].

Several mechanisms have been proposed, including genetic disposition, presence of myocardial bridging of the left anterior descending artery, and mid-cavitary obstruction causing elevated pressures leading to myocardial fibrosis. The true mechanism of aneurysmal formation is likely multifactorial, as each of the above characteristics has been shown to occur in a small minority of patients [37]. Mid-ventricular hypertrophic obstructive cardiomyopathy (HOCM) is characterized by asymmetric left ventricular hypertrophy and by a pressure gradient between basal and apical sites in the left ventricle. These patients are often symptomatic and prone to ventricular arrhythmias arising from the distal left ventricular aneurysm (Fig. 16.13).

Recent evidence shows that adverse event rates in the subgroup with apical aneurysms are substantial at ~10 % per year, including sudden death, ICD discharges, nonfatal thromboembolic stroke, progressive heart failure, and death [37]; thus, patients with apical aneurysms are considered a high-risk subgroup. Often, fibrosis can extend from the aneurysm to the periapical regions in the septum and free wall and may thus serve as a substrate for malignant dysrhythmias [38]. Patients should be considered for ICD implantation for primary prevention of sudden death, particularly those with extensive LGE [10]. Dyskinetic and akinetic segments may harbor pools of stagnant blood flow, leading to the formation of intracavitary thrombi and subsequent thromboembolic

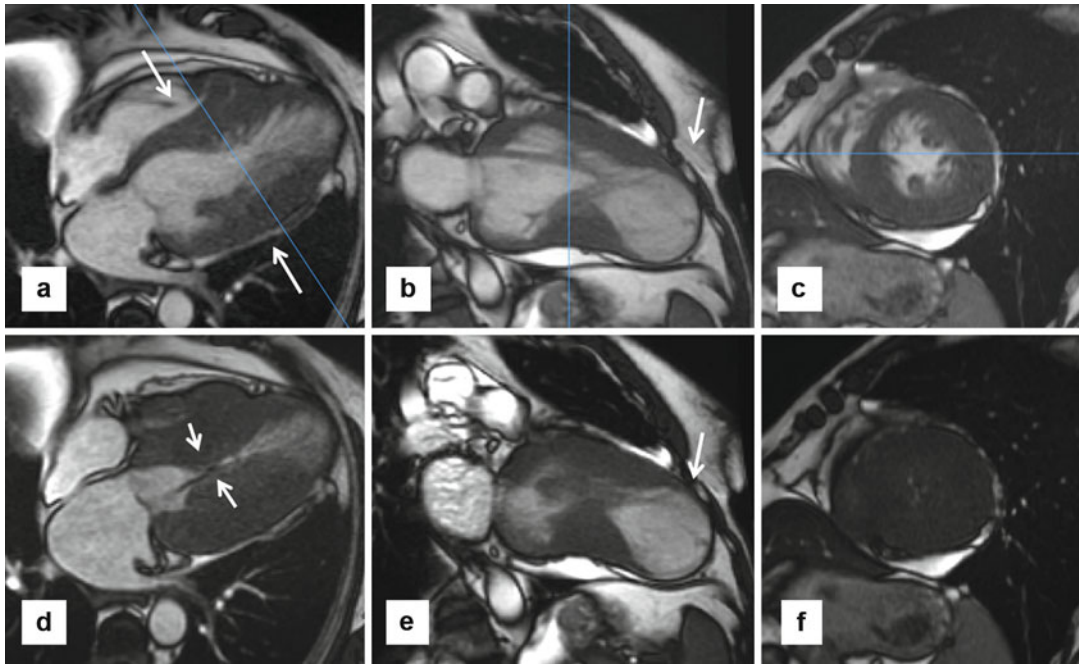

Fig. 16.12 Apical aneurysms. Patients with apical aneurysms represent a small subgroup of high-risk patients. Several mechanisms for aneurysm development have been proposed, including mid-cavitary obstruction. These series of steady state free precession (SSFP) images are from a patient with harsh systolic murmur and shortness of breath, diagnosed with hypertrophic cardiomyopathy with apical aneurysm and mid-cavitary obstruction, with intraventricular gradient >80 mmHg by echocardiogram. (**a**–**c**) Are diastolic and (**d**–**f**) are systolic views. 4-chamber slice (**a**) shows dramatic mid-ventricular hypertrophy (*arrows*) at end diastole and near obliteration of mid-cavity at systole with a jet of dephased blood (*arrows* in **d**) indicative of turbulent flow. 2-chamber views in systole (**b**) and diastole (**e**) showing noncontractile large apical aneurysm (*arrows*). Late gadolinium enhancement imaging did not show any evidence of enhancement, refuting the hypothesis that myocardial fibrosis and subsequent dilation is the mechanism of aneurysm formation

strokes. Among those with a sizable apical aneurysm, there may be a potential role for anticoagulation for stroke prophylaxis.

Fortunately, ventricular rupture is not common despite marked thinning of the myocardium at the apex; thus, prophylactic surgical resection is not warranted.

Tissue Characterization

Late Gadolinium Enhancement (LGE)

Current risk stratification algorithms for sudden cardiac death (SCD) in HCM are imprecise and not always definitive, as SCD occasionally occurs in patients without conventional risk factors (Fig. 16.14). Identification of additional markers to allow more precise selection of those patients who may benefit from primary prevention ICD therapy represents a major clinical aspiration in HCM. Recently, contrast-enhanced CMR with late gadolinium enhancement (LGE) has emerged as an imaging technique to noninvasively identify myocardial fibrosis in coronary artery disease and other cardiomyopathies, including HCM. The prognostic value of LGE in HCM patients has been the subject of immense interest since the first large study demonstrated a possible association between LGE and adverse events [39–44].

Pathophysiology of LGE

Myocardial fibrosis may be a manifestation of the repair process emanating from microvascular

Fig. 16.13 Enhancing apical aneurysm. A young patient with hypertrophic cardiomyopathy and apical aneurysm presented with a recent stroke (presumed to be cardioembolic). (**a**, **b**) Focal hypertrophy in the mid-left ventricle (*arrows*), with a dyskinetic apical aneurysm. Corresponding late gadolinium enhancement (LGE) images on similar planes (**c**, **d**) show substantial enhancement of the left ventricle apex and the periapical regions (*arrows*)

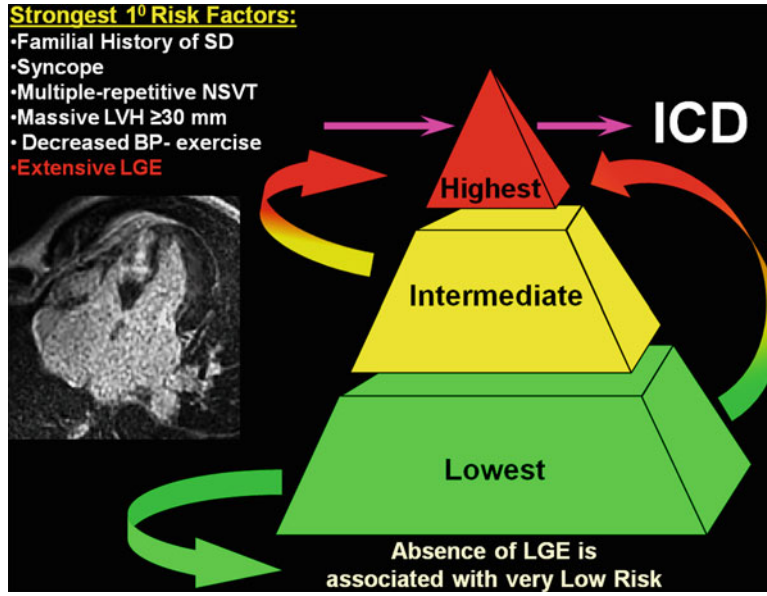

Fig. 16.14 Contrast-enhanced CMR with late gadolinium enhancement can be an arbitrator for implantable cardioverter-defibrillator (*ICD*) placement decisions in HCM patients whose risk remains ambiguous after assessment with conventional risk factors such as a familial history of sudden death, history of unexplained syncope, multiple episodes on non-sustained ventricular tachycardia, massive left ventricular hypertrophy (*LVH*), and abnormal blood pressure response to exercise. Furthermore, extensive late gadolinium enhancement (*LGE*) by itself can identify HCM patients at increased sudden death risk, in whom prophylactic ICD therapy would otherwise not be considered. Conversely, the absence of LGE is associated with low risk of sudden death (*SD*) and therefore a potential source of reassurance to patients. *NSVT* non-sustained ventricular tachycardia

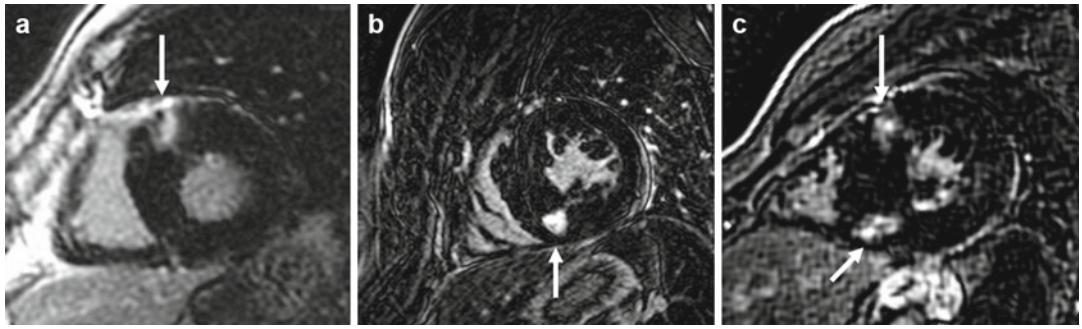

Fig. 16.15 Short-axis slices of late gadolinium enhancement (LGE) imaging, showing the classical "insertion point" enhancement described in various cardiomyopathies, including HCM. (**a**) Prominent LGE seen in isolation at the anterior RV insertion point (*arrow*), (**b**) at the inferior insertion point (*arrow*), and (**c**) at both the anterior and inferior insertion points (*arrows*)

dysfunction and silent ischemia in a large proportion of HCM patients. It has been postulated that LGE mostly represents such areas of myocardial fibrosis. However, much of the histopathological correlations with LGE imaging have been extrapolated from CMR-based animal models involving myocardial infarctions [45]. Only a small number of case reports with explanted end-stage HCM patients [44, 46] and small case series of patients who underwent myectomies [47, 48] have provided direct comparison of LGE to histopathology in HCM. Furthermore, it has been shown that the junction of the septum and right ventricular walls (the so-called RV insertion points) may in fact be areas of expanded extracellular space due to intersecting myocardial fibers rather than myocardial fibrosis (Fig. 16.15) [49]. There is currently no suitable HCM animal model available for study. Thus, the precise mechanism by which LGE occurs in HCM is still uncertain [50], but there is strong circumstantial evidence to support the paradigm of LGE representing areas of replacement fibrosis, particularly in end-stage HCM.

Pattern and Distribution of LGE

Prevalence of LGE is high, with a range between 40 and 80 % depending on patient population. Almost any pattern, distribution, and location of LGE can be observed in HCM (Fig. 16.16). Most commonly, it occurs in a patchy mid-wall distribution, usually involving segments with greatest degrees of hypertrophy [40, 44]. This is likely reflective of the severity of chronic microvascular ischemic damage leading to replacement fibrosis. Patients with greater maximal wall thickness and LV mass index tend to have greater extent of LGE [40, 44] (Fig. 16.17). LGE can be commonly localized to the RV insertion points, likely secondary to myocyte disarray and expansion of extracellular space rather than fibrosis (Fig. 16.15) [49]. As well, LGE can be found in the right ventricular wall and papillary muscles (Fig. 16.10). There is a strong inverse relationship between LVEF and the extent of LGE. Patients with end-stage HCM with depressed ejection fraction usually have extensive LGE seen in all segments (Fig. 16.18) [40, 44, 51]. LGE should not correspond to a coronary vascular distribution, unless there is concomitant coronary artery disease.

As the quantity of LGE may be small, contiguous stacks without gaps are needed to ensure proper sensitivity for small regions of enhancement. At a minimum, three orthogonal planes should be obtained: a short-axis stack with slice thickness of not more than 10 mm, 2-chamber view, and 4-chamber view. High-resolution (voxel size $\leq$1.4 mm) isotropic sequences can also be used if locally available and of sufficient image quality. Furthermore, it is crucial to cross-reference areas of enhancement simultaneously using scanlines in different imaging planes (Fig. 16.17) to exclude artifacts from blood pool and partial volume averaging, particularly in the

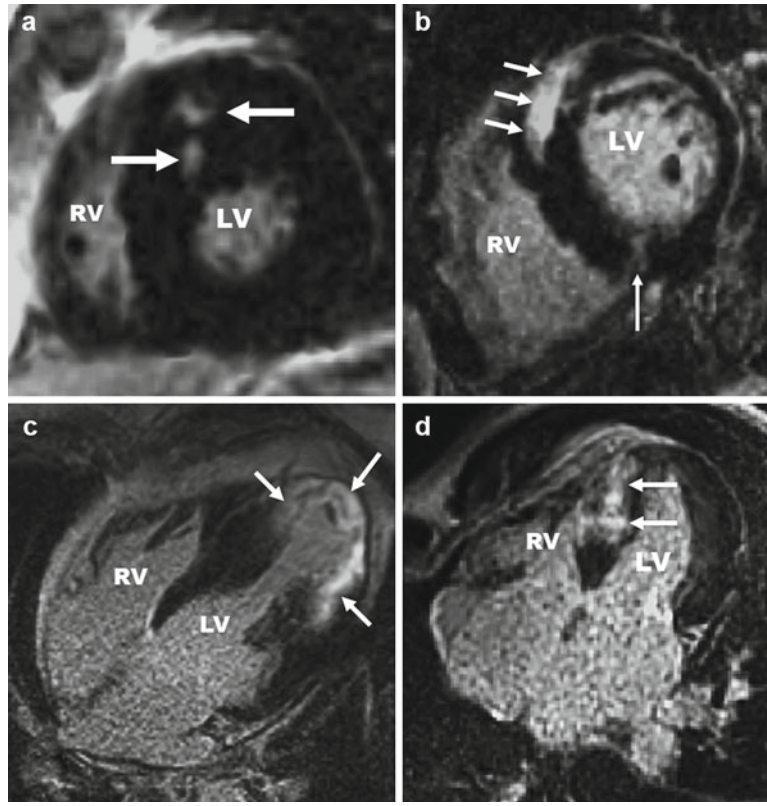

Fig. 16.16 Late gadolinium enhancement (LGE) patterns. Almost any pattern, distribution, and location of LGE can be observed in HCM. (**a**) Basal left ventricle (*LV*) short-axis image from an asymptomatic 29-year-old man with no conventional risk factors and focal areas of LGE confined to mid-myocardial anterior wall (*arrows*), encompassing 4 % of LV mass. (**b**) Mid-LV short-axis image from a 61-year-old woman, with substantial LGE (23 % of LV mass) involving basal anterior septum and contiguous anterolateral free wall (*thick arrows*) as well as a focal area at the intersection of the RV free wall and posterior septum (*thin arrow*). A short five beat run of NSVT on 24-h ambulatory Holter ECG was the only evidence for increased sudden death risk. Extensive LGE acted as an arbitrator for the decision to implant an ICD for primary prevention, which terminated an episode of rapid ventricular tachycardia 5 months later. (**c**) 4-chamber long-axis image from a mildly symptomatic 54-year-old man without conventional sudden risk factors, normal ejection fraction (60 %), and extensive, transmural LGE involving the distal posterior septum, apex, and lateral free wall (*arrows*) encompassing 36 % of LV mass. One year after implantable cardioverter-defibrillator (ICD) placement, this patient received an appropriate ICD shock for rapid monomorphic ventricular tachycardia. (**d**) 4-chamber long-axis image from a 29-year-old man with extensive LGE involving large portions of ventricular septum (*arrows*) encompassing 32 % of LV mass. Over the follow-up period, he developed the end-stage phase of HCM (EF <50 %) associated with progressive heart failure symptoms (NYHA class III), currently under consideration for heart transplantation

basal and apical areas. It is often helpful to use SSFP cine images as another source of reference, due to its high image contrast between dark myocardium and bright blood pool.

LGE and Risk of Adverse Events

Previous studies demonstrated that LGE is associated with ventricular arrhythmias [39–44]. LGE was shown to be an independent predictor of non-sustained ventricular tachycardia (NSVT), even after adjusting for age and maximal wall thickness [52]. These data suggest that LGE may be representative of the burden of arrhythmogenic substrate and perhaps contribute to the risk of lethal arrhythmias in HCM. This is supported by evidence that the presence of NSVT is associated with higher risks of sudden death, particularly in young patients [53].

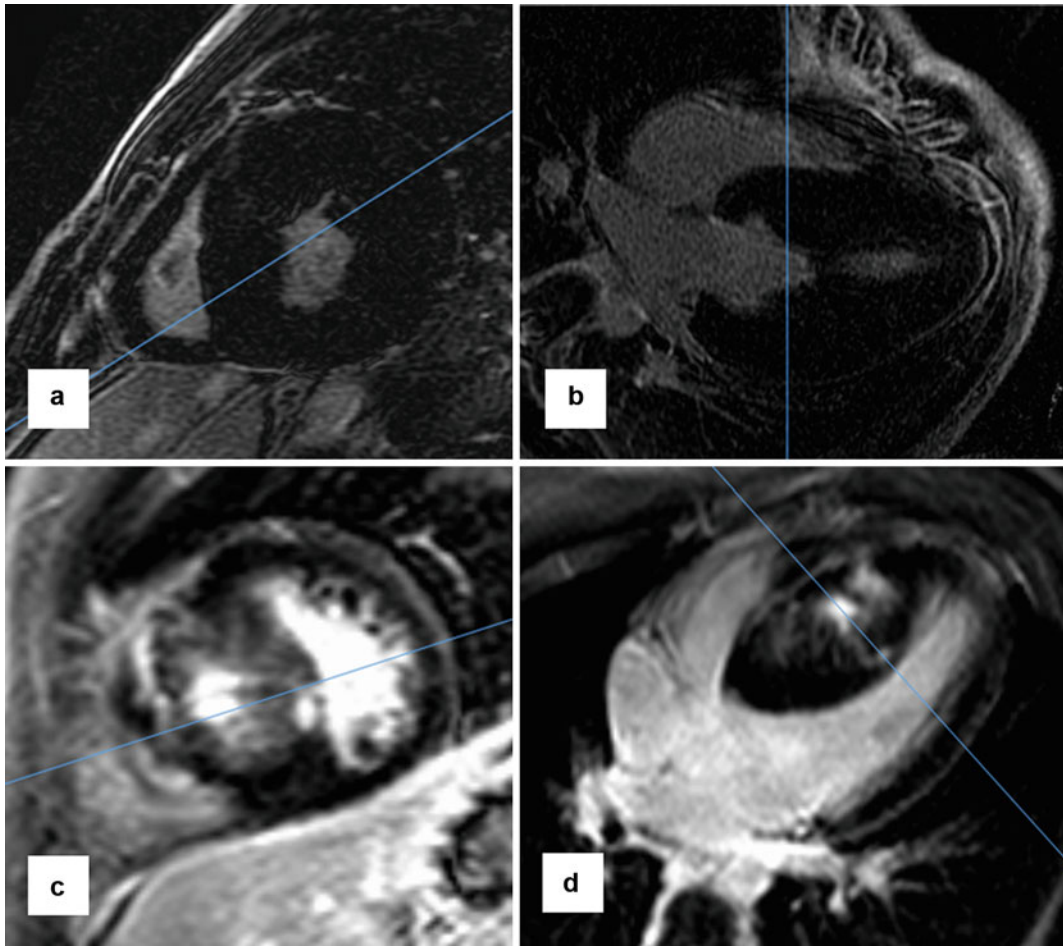

Fig. 16.17 Two patients with extreme hypertrophy, one with late gadolinium enhancement (LGE) and one without. (**a**, **b**) Late gadolinium enhancement imaging of patient with extreme hypertrophy with maximal wall thickness of 31 mm and LV mass of 481 g surprisingly shows complete lack of enhancement in short-axis slices (**a**), confirmed with 4-chamber (**b**) slice. (**c**, **d**) Second patient with extreme hypertrophy with maximal wall thickness of 44 mm and LV mass of 268 g showing extensive LGE in the short-axis slice (**a**) and 4-chamber slice (**b**). The LGE was seen in 33 g or 12 % of the LV mass

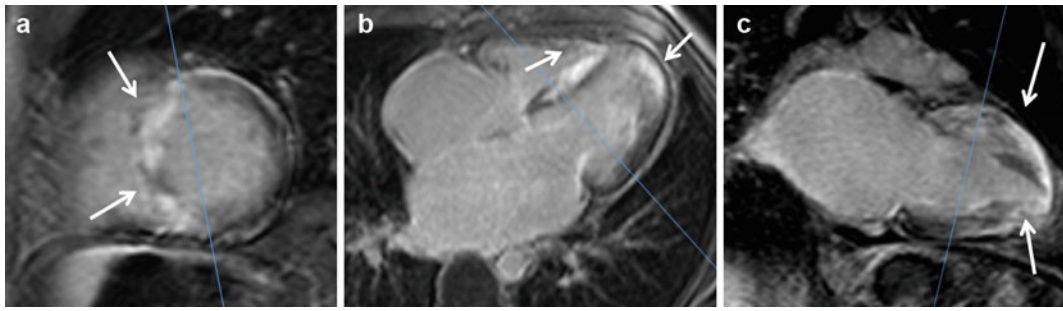

Fig. 16.18 Patients with end-stage HCM usually have extensive late gadolinium enhancement (LGE). In this end-stage HCM patient, late gadolinium enhancement imaging shows extensive enhancement encompassing well over 70 % of the entire LV myocardium. *Scanlines* indicate levels of corresponding slices. (**a**) Short-axis basal-mid-slice showing septum almost completely consisting of enhanced myocardium (*arrows*). (**b**) 4-chamber view shows enhancement in the RV and LV apices (*arrows*). (**c**) 2-chamber view shows enhancement of entire anterior wall and apex (*arrows*)

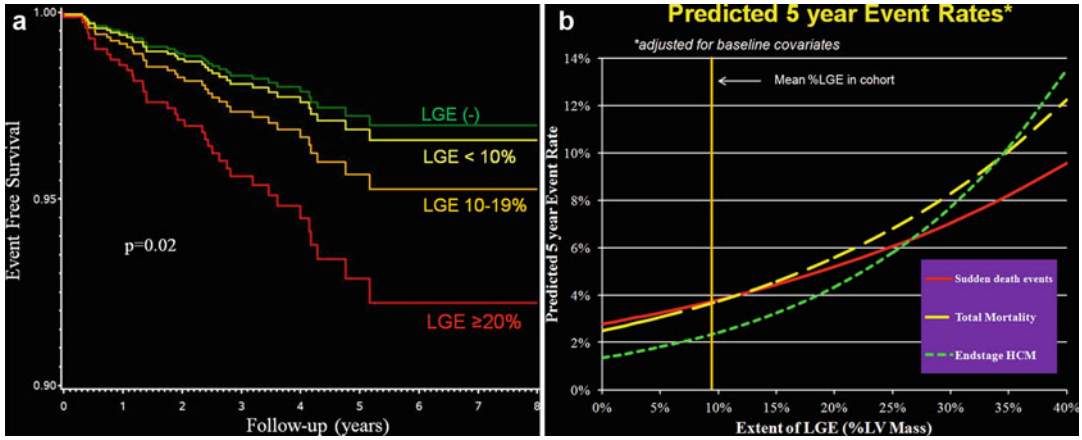

Fig. 16.19 (**a**) Predicted risk of sudden cardiac death events, stratified by the extent of late gadolinium enhancement (*LGE*). The extent of LGE is independently related to risk of sudden cardiac death events in HCM, even after adjusting for baseline risk factors and relevant covariates. (**b**) Risk of adverse events has a continuous independent relationship with the extent of LGE, including sudden death, development of end stage, and total mortality, even after adjusting for relevant baseline covariates

This has generated interest that LGE could serve as a novel risk marker for sudden death, thus improving current risk stratification strategies. Only four small short-term studies have examined the relationship between LGE and sudden death or appropriate therapy for ventricular tachycardia/fibrillation. However, all of the individual studies were underpowered to detect a significant relationship with sudden cardiac death, even when data were combined. It is important to note that these studies have focused entirely on the association between the *presence* of LGE and sudden death. However, the mere presence of any amount of LGE as a binary variable cannot practically be regarded as a risk marker, given that the reported prevalence of some LGE is up to 80 % of all HCM patients. Furthermore, this designation gives equal weight to LGE across a broad spectrum of amounts, from minimal to extensive.

More recently, results from a large prospective cohort study revealed a robust continuous relationship between the amount of LGE and sudden death risk in HCM patients with (as well as without) conventional risk factors (Fig. 16.19a) [51]. The absence of LGE itself was associated with low risk of SCD, representing a potential source of reassurance to patients with no other marker of increased risk. The data provides support for extensive LGE to be an independent prognostic marker for sudden death. The extent of LGE can also be used as an arbitrator in ICD decisions in patients in whom risk stratification remains ambiguous in the presence of possible conventional risk factors (Fig. 16.14). Furthermore, the extent of LGE also predicted development of end-stage HCM and all-cause mortality (Fig. 16.19b).

Intermediate signal-intensity LGE is thought to represent areas of tissue of heterogeneity, where there are islands of myocardium separated by fibrosis. This may potentially be important as these regions have been hypothesized to represent a more arrhythmogenic substrate, making one more likely to experience lethal arrhythmias [54]. While there is an association with ambulatory ventricular tachyarrhythmias in HCM [55], intermediate signal-intensity LGE does not appear to be a superior predictor for identifying high-risk patients for sudden death when compared with visually quantified or high-signal-intensity (i.e., >6 SD above normal mean SI of nulled myocardium) LGE (Fig. 16.20) [56]. The emergence of novel CMR techniques such as T1 mapping may provide an even more precise characterization of abnormal myocardial substrate in HCM [57].

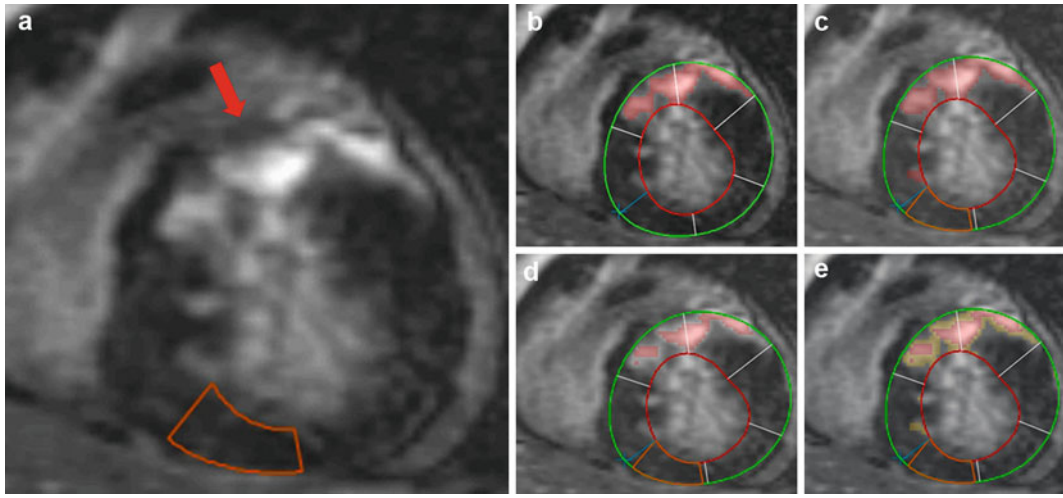

Fig. 16.20 These series of images illustrate the method to which intermediate signal-intensity (or "gray zone") enhancement is identified and quantified. (**a**) Mid-ventricular short-axis late gadolinium enhancement (LGE) image of 36-year-old man with considerable hyperenhancement (*red arrow*) in ventricular septum and anterior wall and a region of interest in normal myocardium (ROI; *orange box*) used to define thresholds for LGE. (**b**) Manual contouring of endocardial border (*red line*) and epicardial border (*green line*) of LV to define myocardium. *Red shading* denotes visually determined area of hyperenhancement. (**c**) Grayscale threshold ≥4SDs above signal intensity (SI) of the ROI (*red shading*), which includes both high- and intermediate-SI LGE. (**d**) High-SI LGE (*red shading*), defined by ≥6SD above SI of the ROI. (**e**) Intermediate-SI LGE (*yellow shading*), identified by subtracting LGE ≥4SD from ≥6SD (superimposed *red shading*)

Stress Perfusion CMR

CMR can be used to assess perfusion deficits and abnormalities of coronary blood flow [58]. Microvascular dysfunction has been well described in this disease and can be evaluated using multiparametric imaging with CMR [59]. It has been shown that ischemia identified by SPECT is associated with increased risk in HCM [60, 61]. Stress perfusion CMR may thus be considered as a further risk stratification tool; however, its role in the overall risk stratification strategy remains undetermined.

Differentiation of Athlete's Heart with HCM

A common clinical problem arises where physiological changes in the hearts of young competitive athletes may overlap phenotypically with a mild expression of HCM. This distinction is particularly important since HCM is the most common cause of sudden death in young competitive athletes [62]. Of these deaths, the vast majority occur during periods of severe exertion during training or competition. Accurate diagnosis has profound implications, as the misdiagnosis of disease may unnecessarily disqualify a patient from further participation and competition. On the other hand, proper identification of athletes with HCM can form the basis for disqualification from certain types of athletic activities in order to minimize risk.

Long-term athletic training (particularly in high-intensity endurance sports such as distance running, cycling, swimming, and rowing) can lead to increases in LV wall thickness, along with increases in LV end-diastolic volumes which leads to an increase in LV mass [63]. During such activities, cardiac output is greatly increased through physiological elevations in heart rate, stroke volume, and blood pressure, with a concomitant reduction in peripheral vascular resistance. Subsequently, the heart is subjected to predominantly a volume load, rather than a pressure load as experienced during

Table 16.1 Characteristics of athlete's heart versus hypertrophic cardiomyopathy (HCM)

Characteristic	Athlete's heart	HCM
LV end-diastolic dimension >55 mm	Present (>1/3 of highly trained elite male athletes), particularly in endurance athletes	Uncommon until the end stage with heart failure and systolic dysfunction
LV end-diastolic dimension <45 mm	Inconsistent with athlete's heart	If present, is supportive of diagnosis
Focal or "unusual" patterns of hypertrophy	Absent	Common
Degree of hypertrophy	Normal or mildly increased (≤12 mm), <2 % may be up to 16 mm	Average thickness ~20 mm, with small subgroup with substantial thickening >50 mm
Decreased thickness (~2–5 mm) within 3 months of deconditioning	Supportive of diagnosis	Absent
Left atrial enlargement	Absent	May be present
Peak oxygen consumption (VO_2) >110 %	Present	Absent
Late gadolinium enhancement	May be present, usually in small amounts in mid-myocardium and at RV insertion points, never extensive	Common (40–60 %), may be at RV insertion points but also elsewhere, occasionally (~10 %) extensive
Sarcomeric mutation on genetic testing	Absent	May be present (~40–50 %)
Family history of HCM	Absent	May be present
Abnormal ECG	May be present, thus not helpful	May be present
Right ventricular involvement	Absent	Occasionally present
Transmitral filling pattern on echocardiography	Normal	Decreased E wave, increased A wave, or may be normal

LV left ventricle, *RV* right ventricle, *ECG* electrocardiogram

isometric exercises such as weight lifting [64], thus leading to cavitary dilation. However, athletes engaging in either form of exercise tend to have increased LV cavity size compared with controls, a characteristic that is helpful in differentiating an athlete's heart from HCM, where cavity sizes tend to be small. Pathological changes such as severe left atrial enlargement and LV systolic and diastolic dysfunction should not occur in athlete's heart.

Cessation of systemic training in the athlete over a period of several months will cause regression of increased wall thickness but will not result in regression of hypertrophy in patients with HCM [65]. This method has been advocated as a method of differentiating between athlete's heart and HCM, since there should be no expected regression with detraining in true cardiac disease. Furthermore, the presence of greater than small amounts of LGE is highly suggestive of HCM and not athlete's heart.

Table 16.1 Lists of helpful findings which can help distinguish between athlete's heart and HCM

Differentiation of Hypertensive Heart Disease with HCM

A frequent diagnostic dilemma occurs when a patient with suspected HCM also has concomitant hypertension (Fig. 16.21). Typically, chronic hypertension produces concentric remodeling rather than asymmetric septal hypertrophy (ASH), although ASH is frequently encountered in elderly patients. Patients with a family history of HCM, ventricular hypertrophy in a nonhypertensive relative, or a positive genetic test may be supportive of a diagnosis of HCM. Treatment of hypertension may regress hypertrophy in those with hypertension. Hypertension rarely produces wall thickness >18 mm, while the average LV wall thickness in HCM is 21 mm. Strain metrics

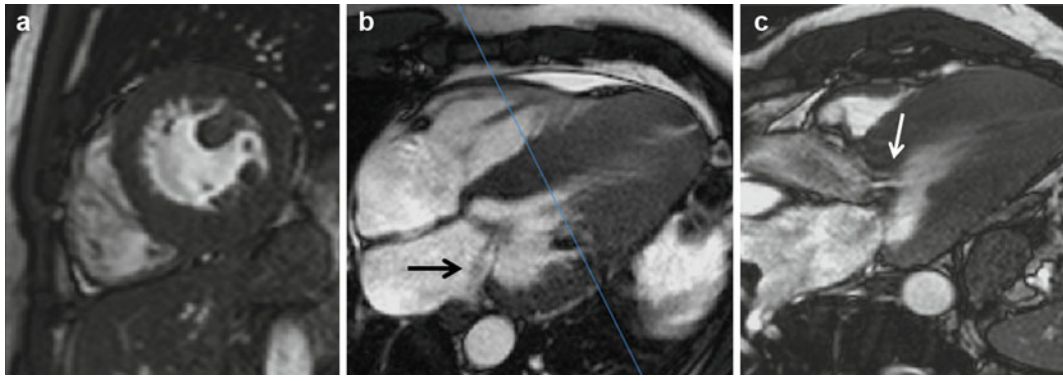

Fig. 16.21 Patient with genotype-positive HCM with concomitant hypertension. (**a**) Short-axis slice shows concentric thickening, with enlarged papillary muscle. (**b**) 4-chamber view shows a dephased jet of blood consistent with posteriorly directed mitral regurgitation (*arrow*). Note prominent hypertrophy in the apical region. *Scanline* represents level of the short-axis slice. (**c**) 3-chamber view in systole shows dephasing through left ventricle outflow tract (*arrow*), representing flow acceleration originating mitral leaflet tip secondary to chordal systolic anterior motion

from echocardiography and CMR are emerging as novel discriminatory tools [66–68].

Certain patterns of septal hypertrophy may be more prominent in HCM, such as reverse curvature and apical hypertrophy. Other patterns such as a sigmoid shape are more prominent in elderly hypertensive patients [69] and have been shown to be negative predictor of HCM genotype [70]. It also has to be noted that there may be significant overlap in phenotypes; therefore, diagnosis of hypertension does not necessarily preclude the diagnosis of HCM.

Differentiation of Metabolic and Infiltrative Cardiomyopathies and HCM

A variety of genetic diseases can produce phenotypes that may have myocardial geometry similar to HCM. The most common "non-sarcomeric" diseases include cardiac amyloidosis, Anderson-Fabry's disease, and Danon disease. Generally, most of these conditions produce symmetric rather than asymmetric hypertrophy, and LVOT obstruction is less common.

A systematic approach, including obtaining an accurate and complete family history, symptoms, physical examination, judicious use of imaging, and biochemical and genetic testing, is vital to the differential diagnosis between such diseases and hypertrophic cardiomyopathy. For example, CMR imaging can be used to identify patterns of LVH and LGE which can raise suspicion for diagnosis of HCM phenocopies. Molecular diagnosis can then be used as confirmatory tests for Danon and Fabry's disease, while biopsy should be considered for amyloid.

Anderson-Fabry's disease is an x-linked lysosomal storage disease where mutations in the α-galactosidase A gene lead to accumulation of glycosphingolipids in multiple organs, including the kidneys and heart. Cardiac manifestations are serious and progressive and may include left ventricular thickening, conduction abnormalities, dysrhythmias, and valve disease and are not usually detected until the third or fourth decade of life. Cardiac diseases are a major cause of death in patients with Fabry's [71]. Adults with this disease have LGE most commonly localized to the basal inferolateral wall, which would be an unusual distribution in HCM.

Danon disease is another x-linked lysosomal storage disease where mutations in the lysosome-associated membrane protein 2 (LAMP2) cause skeletal myopathy, developmental delay, and cardiomyopathy. Patients may present during adolescence with elevated creatine kinase, preexcitation pattern on ECG, left ventricular hypertrophy, and retinitis pigmentosa. Most patients die rapidly from

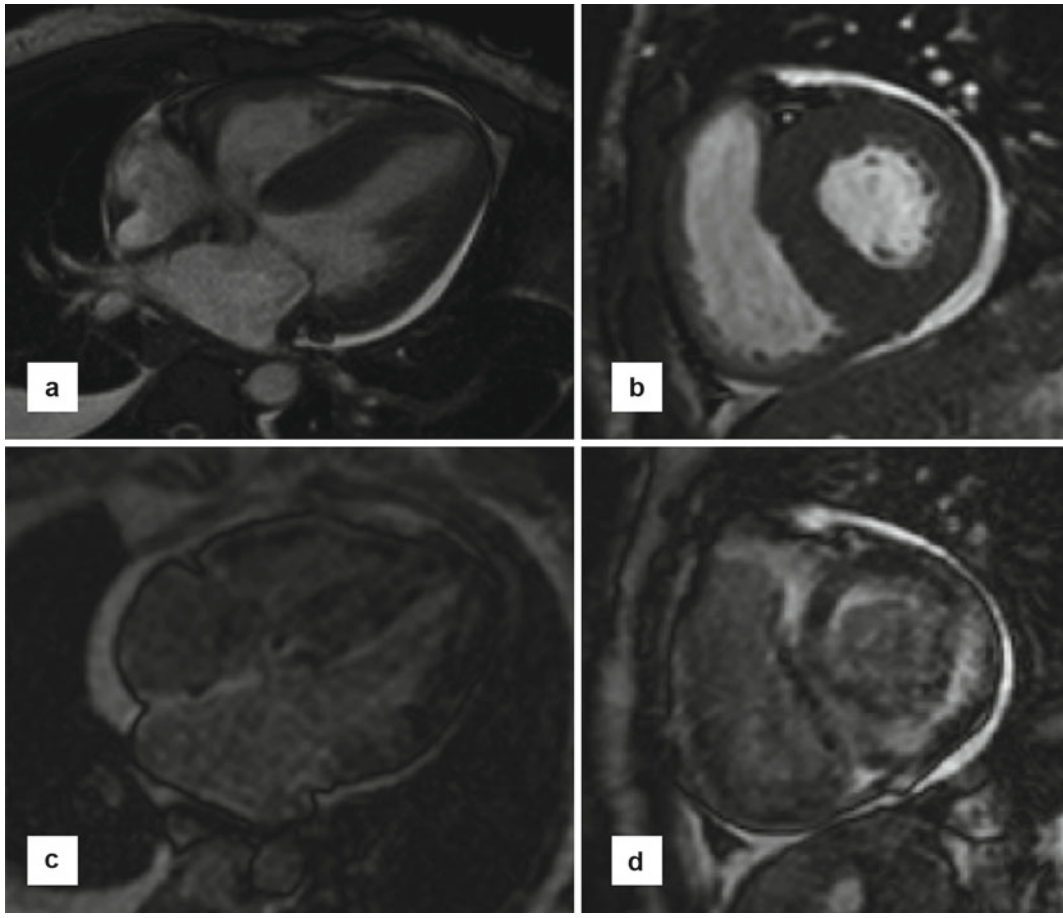

Fig. 16.22 Patient with biopsy-proven AL cardiac amyloidosis, showing several classical MR findings of amyloidosis. (**a**) 4-chamber steady state free precession (SSFP) showing diffuse thickening of LV myocardium and enlarged left atrium. Note small circumferential pericardial effusion and mild bilateral pleural effusions. (**b**) Short-axis SSFP slice showing symmetric thickening and small pericardial effusion. (**c**) Look-Locker T1 scout showing the typical "failure to null" appearance of myocardium despite varying inversion times from 100 to 500 ms. (**d**) Short-axis late gadolinium enhancement (LFE) imaging showing diffuse LGE as well as regions of subendocardial enhancement not in typical coronary distribution

heart failure (typically <25 years old), with a small proportion dying from sudden cardiac death [72].

Mutations in PRKAG2, the γ2 subunit of AMP-activated protein kinase (AMPK), can cause a syndrome of HCM, conduction abnormalities, and Wolff-Parkinson-White syndrome. However, this mutation does not seem to result in malignant consequences, such as sudden death and ventricular dilation [73].

Amyloidosis is caused by the abnormal deposition of insoluble amyloid proteins throughout the body, with cardiac involvement being more frequent in the AL and TTE subtypes. Amyloid deposition leads to diastolic dysfunction and restrictive cardiomyopathy, which ultimately progresses to heart failure. It is the leading cause of death for patients with AL amyloidosis. CMR shows a characteristic "failure to null" pattern in T1 scout during late gadolinium enhancement imaging, together with abnormal blood pool gadolinium kinetics. Patients may exhibit a pattern of global subendocardial LGE or patchy focal involvement in the LV myocardium. Supportive findings include enlarged atria (likely secondary to restrictive cardiomyopathy), pericardial effusion, and pleural effusions (Fig. 16.22).

Left Ventricular Noncompaction (LVNC)

Left ventricular noncompaction, or LVNC, was first reported in 1984 (Fig. 16.23) [74]. It was initially observed in echocardiography with the appearance of persistent myocardial sinusoids. Its prevalence is estimated to be between 0.05 and 0.24 %, with a wide range of ages at presentation with no predilection for any specific age [75]. Over half of all cases are male.

LVNC is hypothesized to be due to abnormal compaction of the myocardium during the fifth and eighth week of embryonic development. The trabecular layer of the ventricle has been observed to compact from the base to apex during development, from epicardium to endocardium, and from the septal to lateral wall. However, cases of acquired LVNC have been described, where infants whose echocardiograms did not show LVNC but were subsequently diagnosed with the disease later in life [76, 77].

Different genes found to be associated with LVNC include taffazin, β-dystrobrevin (DTNA), Cypher/ZASP (LDB3), lamin A/C (LMNA), SCN5A, MYH7, and MYBPC3 [78]. Much like HCM, there is considerable genetic heterogeneity associated with LVNC. As well, LVNC can exist concurrently with HCM or dilated cardiomyopathy [79]. Familial involvement ranges

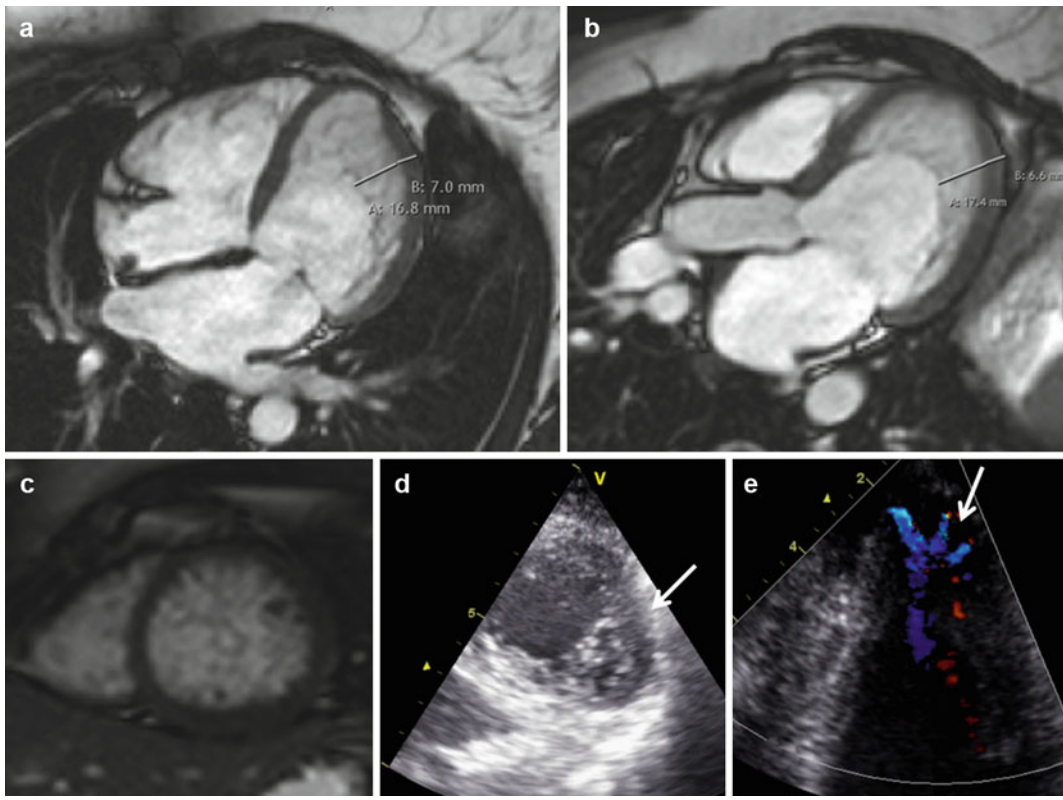

Fig. 16.23 Patient with suspected noncompaction on echocardiography. (**a**) 4-chamber slice shows large area of noncompacted myocardium, with a thickness ratio of 16.8/7 = 2.4 in relation to adjacent myocardium during diastole. (**b**) 3-chamber view of the same patient with a thickness ratio of 17.4/6.6 = 2.6. A maximum diastolic ratio of noncompacted versus compacted myocardium of >2.3–2.5 is required in three long-axis views. (**c**) Short-axis slice near the apex shows noncompacted myocardium filling the entire LV cavity. (**d**) Short-axis echocardiography near the apex shows echo-lucent matrix-like structure suggestive of noncompacted myocardium. (**e**) Color Doppler in 4-chamber orientation helps highlight blood flow in the recesses. There appear to be numerous prominent trabeculations with deep intertrabecular spaces. Alternatively, contrast echocardiography can be used

from 18 to 33 % [80–82]. Current guidelines recommend clinical screen of first-degree relatives of probands; however, genetic testing is not routinely recommended [83].

Echocardiography is the initial diagnostic test of choice, with contrast echo, transesophageal echo, and three-dimensional echo serving as useful adjuncts. There is no clear consensus on the echocardiographic diagnostic criteria for LVNC, as each threshold will have different sensitivities and specifies. The three most widely used criteria include:

1. Jenni criteria [84]: In parasternal short-axis view, end-*systolic* ratio >2 of noncompacted to compact layer; the absence of other coexisting structural abnormalities, plus numerous excessively prominent trabeculations and deep intertrabecular spaces; and recesses perfused by intraventricular blood seen by color Doppler
2. Chin criteria [85]: In parasternal short-axis view or apical views, end-*diastolic* ratio of compact layer to total thickness of LV <0.5
3. Stollberger criteria [75]: >3 trabeculations protruding from the LV free wall apically to the papillary muscles seen on one imaging plane; intertrabecular spaces perfused from the LV cavity shown by color Doppler

Different criteria have also been proposed, including combining the Jenni and Stollberger criteria or by quantifying along a continuum the noncompacted/compacted ratio and areas of noncompaction [86, 87].

Due to lower spatial resolution of echocardiography, and in its often suboptimal characterization of apical segments (where noncompacted areas are most commonly found), LVNC often goes undiagnosed or misdiagnosed as HCM or dilated cardiomyopathy. The superior image resolution and unlimited imaging planes make CMR a complementary (and often superior) tool in establishing the diagnosis. The Petersen criteria [88] in CMR require an end-*diastolic* ratio >2.3 of trabecular and compact layers (Fig. 16.23). These criteria have been shown to have high diagnostic accuracy to distinguish pathological LVNC from noncompaction seen in healthy, dilated, and hypertrophied hearts. Cardiac CT and contrast left ventriculography can also be useful if there is a need for concurrent delineation of coronary anatomy.

Asymptomatic patients do not need treatment but need to be followed, but all symptomatic patients should be followed closely. Incidence of NYHA class II/IV heart failure ranges from 35 to 44 % [80, 89]. Treatment of patients include medical therapy with beta-blockers, ACE inhibitors, and diuretics in those with systolic dysfunction [90]. Cardiac resynchronization therapy with or without an ICD is recommended for those on optimal medical therapy with LVEF <35 % and QRS >0.120 s [91]. Patients should also be monitored for ventricular arrhythmias, with ICD implantation in the appropriate patients. Prognosis depends on symptoms and LV ejection fraction.

References

1. Maron BJ, Maron MS, Semsarian C. Double or compound sarcomere mutations in hypertrophic cardiomyopathy: a potential link to sudden death in the absence of conventional risk factors. Heart Rhythm. 2012;9(1):57–63.
2. Konno T, Chang S, Seidman JG, Seidman CE. Genetics of hypertrophic cardiomyopathy. Curr Opin Cardiol. 2010;25(3):205–9.
3. Judge DP. Use of genetics in the clinical evaluation of cardiomyopathy. JAMA. 2009;302(22):2471–6.
4. Maron BJ, Maron MS. Hypertrophic cardiomyopathy. Lancet. 2013;381:242–55.
5. Maron BJ. Hypertrophic cardiomyopathy: an important global disease. Am J Med. 2004;116(1):63–5.
6. Olivotto I, Maron MS, Adabag S, et al. Gender-related differences in the clinical presentation and outcome of hypertrophic cardiomyopathy. J Am Coll Cardiol. 2005;46(3):480–7.
7. Maron BJ. Hypertrophic cardiomyopathy: a systematic review. JAMA. 2002;287(10):1308–20.
8. Teare D. Asymmetrical hypertrophy of the heart in young adults. Br Heart J. 1958;20(1):1–8.
9. Gersh BJ, Maron BJ, Bonow RO, et al. 2011 ACCF/AHA guideline for the diagnosis and treatment of hypertrophic cardiomyopathy: executive summary: a report of the American College of Cardiology Foundation/American Heart Association Task Force on Practice Guidelines. Circulation. 2011;124(24):2761–96.
10. Chan RH, Maron B, Olivotto I, et al. Prognostic utility of contrast-enhanced cardiovascular magnetic resonance in hypertrophic cardiomyopathy: an International Multicenter Study. J Am Coll Cardiol. 2012;59(13):E1570.

11. Klues HG, Schiffers A, Maron BJ. Phenotypic spectrum and patterns of left ventricular hypertrophy in hypertrophic cardiomyopathy: morphologic observations and significance as assessed by two-dimensional echocardiography in 600 patients. J Am Coll Cardiol. 1995;26(7):1699–708.
12. Maron MS, Maron BJ, Harrigan C, et al. Hypertrophic cardiomyopathy phenotype revisited after 50 years with cardiovascular magnetic resonance. J Am Coll Cardiol. 2009;54(3):220–8.
13. Maron MS, Lesser JR, Maron BJ. Management implications of massive left ventricular hypertrophy in hypertrophic cardiomyopathy significantly underestimated by echocardiography but identified by cardiovascular magnetic resonance. Am J Cardiol. 2010;105(12):1842–3.
14. Rickers C, Wilke NM, Jerosch-Herold M, et al. Utility of cardiac magnetic resonance imaging in the diagnosis of hypertrophic cardiomyopathy. Circulation. 2005;112(6):855–61.
15. Spirito P, Bellone P, Harris KM, Bernabo P, Bruzzi P, Maron BJ. Magnitude of left ventricular hypertrophy and risk of sudden death in hypertrophic cardiomyopathy. N Engl J Med. 2000;342(24):1778–85.
16. Maron MS, Rowin EJ, Lin D, et al. Prevalence and clinical profile of myocardial crypts in hypertrophic cardiomyopathy. Circ Cardiovasc Imaging. 2012;5(4):617–36.
17. Germans T, Wilde AAM, Dijkmans PA, et al. Structural abnormalities of the inferoseptal left ventricular wall detected by cardiac magnetic resonance imaging in carriers of hypertrophic cardiomyopathy mutations. J Am Coll Cardiol. 2006;48(12):2518–23.
18. Olivotto I, Maron MS, Autore C, et al. Assessment and significance of left ventricular mass by cardiovascular magnetic resonance in hypertrophic cardiomyopathy. J Am Coll Cardiol. 2008;52(7):559–66.
19. Maron MS, Hauser TH, Dubrow E, et al. Right ventricular involvement in hypertrophic cardiomyopathy. Am J Cardiol. 2007;100(8):1293–8.
20. Keeling AN, Carr JC, Choudhury L. Right ventricular hypertrophy and scarring in mutation positive hypertrophic cardiomyopathy. Eur Heart J. 2010;31(3):381.
21. Maron BJ, Dearani JA, Ommen SR, et al. The case for surgery in obstructive hypertrophic cardiomyopathy. J Am Coll Cardiol. 2004;44(10):2044–53.
22. Minakata K, Dearani JA, Schaff HV, O'Leary PW, Ommen SR, Danielson GK. Mechanisms for recurrent left ventricular outflow tract obstruction after septal myectomy for obstructive hypertrophic cardiomyopathy. Ann Thorac Surg. 2005;80(3):851–6.
23. Delahaye F, Jegaden O, De Gevigney G, et al. Postoperative and long-term prognosis of myotomy-myomectomy for obstructive hypertrophic cardiomyopathy: influence of associated mitral valve replacement. Eur Heart J. 1993;14(9):1229–37.
24. Kwon DH, Smedira NG, Popovic ZB, et al. Steep left ventricle to aortic root angle and hypertrophic obstructive cardiomyopathy: study of a novel association using three-dimensional multimodality imaging. Heart. 2009;95(21):1784–91.
25. Maron MS, Olivotto I, Betocchi S, et al. Effect of left ventricular outflow tract obstruction on clinical outcome in hypertrophic cardiomyopathy. N Engl J Med. 2003;348(4):295–303.
26. Geske JB, Sorajja P, Ommen SR, Nishimura RA. Left ventricular outflow tract gradient variability in hypertrophic cardiomyopathy. Clin Cardiol. 2009;32(7):397–402.
27. Geske JB, Cullen MW, Sorajja P, Ommen SR, Nishimura RA. Assessment of left ventricular outflow gradient: hypertrophic cardiomyopathy versus aortic valvular stenosis. JACC Cardiovasc Interv. 2012;5(6):675–81.
28. Nagueh SF, Bierig SM, Budoff MJ, et al. American Society of Echocardiography clinical recommendations for multimodality cardiovascular imaging of patients with hypertrophic cardiomyopathy: Endorsed by the American Society of Nuclear Cardiology, Society for Cardiovascular Magnetic Resonance, and Society of Cardiovascular Computed Tomography. J Am Soc Echocardiogr. 2011;24(5):473–98.
29. Kwon DH, Setser RM, Thamilarasan M, et al. Abnormal papillary muscle morphology is independently associated with increased left ventricular outflow tract obstruction in hypertrophic cardiomyopathy. Heart. 2008;94(10):1295–301.
30. Harrigan CJ, Appelbaum E, Maron BJ, et al. Significance of papillary muscle abnormalities identified by cardiovascular magnetic resonance in hypertrophic cardiomyopathy. Am J Cardiol. 2008;101(5):668–73.
31. Minakata K, Dearani JA, Nishimura RA, Maron BJ, Danielson GK. Extended septal myectomy for hypertrophic obstructive cardiomyopathy with anomalous mitral papillary muscles or chordae. J Thorac Cardiovasc Surg. 2004;127(2):481–9.
32. Shapiro LM, McKenna WJ. Distribution of left ventricular hypertrophy in hypertrophic cardiomyopathy: a two-dimensional echocardiographic study. J Am Coll Cardiol. 1983;2(3):43744.
33. Gruner C, Chan RH, Rowin EJ, et al. Left ventricular apico-basal muscle bundle identified by cardiovascular magnetic resonance imaging in patients with hypertrophic cardiomyopathy: implications for diagnosis and management. Circulation. 2012;126(21 Suppl), A14941.
34. Maron MS, Olivotto I, Harrigan C, et al. Mitral valve abnormalities identified by cardiovascular magnetic resonance represent a primary phenotypic expression of hypertrophic cardiomyopathy. Circulation. 2011;70:40–7.
35. Grigg LE, Wigle ED, Williams WG, Daniel LB, Rakowski H. Transesophageal Doppler echocardiography in obstructive hypertrophic cardiomyopathy: clarification of pathophysiology and importance in intraoperative decision making. J Am Coll Cardiol. 1992;20(1):42–52.
36. Fattori R, Biagini E, Lorenzini M, Buttazzi K, Lovato L, Rapezzi C. Significance of magnetic resonance imaging in apical hypertrophic cardiomyopathy. Am J Cardiol. 2010;105(11):1592–6.

37. Maron MS, Finley JJ, Bos JM, et al. Prevalence, clinical significance, and natural history of left ventricular apical aneurysms in hypertrophic cardiomyopathy. Circulation. 2008;118(15):1541–9.
38. Lim K-K, Maron BJ, Knight BP. Successful catheter ablation of hemodynamically unstable monomorphic ventricular tachycardia in a patient with hypertrophic cardiomyopathy and apical aneurysm. J Cardiovasc Electrophysiol. 2009;20(4):445–7.
39. Bruder O, Wagner A, Jensen CJ, et al. Myocardial scar visualized by cardiovascular magnetic resonance imaging predicts major adverse events in patients with hypertrophic cardiomyopathy. J Am Coll Cardiol. 2010;56(11):875–87.
40. Maron MS, Appelbaum E, Harrigan CJ, et al. Clinical profile and significance of delayed enhancement in hypertrophic cardiomyopathy. Circ Heart Fail. 2008;1(3):184–91.
41. Rubinshtein R, Glockner JF, Ommen SR, et al. Characteristics and clinical significance of late gadolinium enhancement by contrast-enhanced magnetic resonance imaging in patients with hypertrophic cardiomyopathy. Circ Heart Fail. 2010;3(1):51–8.
42. O'Hanlon R, Grasso A, Roughton M, et al. Prognostic significance of myocardial fibrosis in hypertrophic cardiomyopathy. J Am Coll Cardiol. 2010;56(11):867–74.
43. Kwon DH, Setser RM, Popovic ZB, et al. Association of myocardial fibrosis, electrocardiography and ventricular tachyarrhythmia in hypertrophic cardiomyopathy: a delayed contrast enhanced MRI study. Int J Cardiovasc Imaging. 2008;24(6):617–25.
44. Moon JCC, McKenna WJ, McCrohon JA, Elliott PM, Smith GC, Pennell DJ. Toward clinical risk assessment in hypertrophic cardiomyopathy with gadolinium cardiovascular magnetic resonance. J Am Coll Cardiol. 2003;41(9):1561–7.
45. Kim RJ, Fieno DS, Parrish TB, et al. Relationship of MRI delayed contrast enhancement to irreversible injury, infarct age, and contractile function. Circulation. 1999;100(19):1992–2002.
46. Papavassiliu T, Schnabel P, Schröder M, Borggrefe M. CMR scarring in a patient with hypertrophic cardiomyopathy correlates well with histological findings of fibrosis. Eur Heart J. 2005;26(22):2395.
47. Moravsky G, Ofek E, WIlliams L, Butany J, Rakowski H, Crean A. Cardiovascular magnetic resonance imaging with late gadolinium enhancement and histopathological correlation in hypertrophic cardiomyopathy. Circulation. 2011;124, A14546.
48. Kwon DH, Smedira NG, Rodriguez ER, et al. Cardiac magnetic resonance detection of myocardial scarring in hypertrophic cardiomyopathy: correlation with histopathology and prevalence of ventricular tachycardia. J Am Coll Cardiol. 2009;54(3):242–9.
49. Kuribayashi T, Roberts WC. Myocardial disarray at junction of ventricular septum and left and right ventricular free walls in hypertrophic cardiomyopathy. Am J Cardiol. 1992;70(15):1333–40.
50. Maron MS. Clinical utility of cardiovascular magnetic resonance in hypertrophic cardiomyopathy. J Cardiovasc Magn Reson. 2012;14(1):13.
51. Chan RH, Maron BJ, Olivotto I, et al. Prognostic utility of contrast-enhanced cardiovascular magnetic resonance imaging in hypertrophic cardiomyopathy: an International Multicenter Study. Circulation. 2012;126(21 Suppl), A13139.
52. Adabag S, Maron BJ, Appelbaum E, et al. Occurrence and frequency of arrhythmias in hypertrophic cardiomyopathy in relation to delayed enhancement on cardiovascular magnetic resonance. J Am Coll Cardiol. 2008;51(14):1369–74.
53. Monserrat L, Elliott PM, Gimeno JR, Sharma S, Penas-Lado M, McKenna WJ. Non-sustained ventricular tachycardia in hypertrophic cardiomyopathy: an independent marker of sudden death risk in young patients. J Am Coll Cardiol. 2003;42(5):873–9.
54. Yan AT, Shayne AJ, Brown KA, et al. Characterization of the peri-infarct zone by contrast-enhanced cardiac magnetic resonance imaging is a powerful predictor of post-myocardial infarction mortality. Circulation. 2006;114(1):32–9.
55. Appelbaum E, Maron BJ, Adabag S, et al. Intermediate-signal-intensity late gadolinium enhancement predicts ventricular tachyarrhythmias in patients with hypertrophic cardiomyopathy. Circ Cardiovasc Imaging. 2012;5(1):78–85.
56. Chan RH, Afilalo J, Maron BJ, et al. Prognostic utility of intermediate-signal-intensity late gadolinium enhancement in patients with hypertrophic cardiomyopathy. Circulation. 2012;126(21 Suppl), A17374.
57. Mewton N, Liu CY, Croisille P, Bluemke D, Lima JA. Assessment of myocardial fibrosis with cardiovascular magnetic resonance. J Am Coll Cardiol. 2011;57(8):891–903.
58. Kawada N, Sakuma H, Yamakado T, et al. Hypertrophic cardiomyopathy: MR measurement of coronary blood flow and vasodilator flow reserve in patients and healthy subjects. Radiology. 1999;211(1):129–35.
59. Petersen SE, Jerosch-Herold M, Hudsmith LE, et al. Evidence for microvascular dysfunction in hypertrophic cardiomyopathy: new insights from multiparametric magnetic resonance imaging. Circulation. 2007;115(18):2418–25.
60. Kaimoto S, Kawasaki T, Kuribayashi T, et al. Myocardial perfusion abnormality in the area of ventricular septum-free wall junction and cardiovascular events in nonobstructive hypertrophic cardiomyopathy. Int J Cardiovasc Imaging. 2012;28(7):1829–39.
61. Sorajja P, Chareonthaitawee P, Ommen SR, Miller TD, Hodge DO, Gibbons RJ. Prognostic utility of single-photon emission computed tomography in adult patients with hypertrophic cardiomyopathy. Am Heart J. 2006;151(2):426–35.
62. Maron BJ, Pelliccia A, Spirito P. Cardiac disease in young trained athletes. Insights into methods for distinguishing athlete's heart from structural heart disease, with particular emphasis on hypertrophic cardiomyopathy. Circulation. 1995;91(5):1596–601.
63. Maron BJ. Structural features of the athlete heart as defined by echocardiography. J Am Coll Cardiol. 1986;7(1):190–203.

64. Morganroth J, Maron BJ, Henry WL, Epstein SE. Comparative left ventricular dimensions in trained athletes. Ann Intern Med. 1975;82(4):521–4.
65. Fagard R. Athlete's heart. Heart. 2003;89(12): 1455–61.
66. Carasso S, Yang H, Woo A, Jamorski M, Wigle ED, Rakowski H. Diastolic myocardial mechanics in hypertrophic cardiomyopathy. J Am Soc Echocardiogr. 2010;23(2):164–71.
67. Kato TS, Noda A, Izawa H, et al. Discrimination of nonobstructive hypertrophic cardiomyopathy from hypertensive left ventricular hypertrophy on the basis of strain rate imaging by tissue Doppler ultrasonography. Circulation. 2004;110(25):3808–14.
68. Saito M, Okayama H, Yoshii T, et al. The differences in left ventricular torsional behavior between patients with hypertrophic cardiomyopathy and hypertensive heart disease. Int J Cardiol. 2011;150(3):301–6.
69. Lever HM, Karam RF, Currie PJ, Healy BP. Hypertrophic cardiomyopathy in the elderly. Distinctions from the young based on cardiac shape. Circulation. 1989;79(3):580–9.
70. Binder J, Ommen SR, Gersh BJ, et al. Echocardiography-guided genetic testing in hypertrophic cardiomyopathy: septal morphological features predict the presence of myofilament mutations. Mayo Clin Proc. 2006;81(4):459–67.
71. Mehta A, Beck M, Eyskens F, et al. Fabry disease: a review of current management strategies. QJM. 2010;103(9):641–59.
72. Arad M, Maron BJ, Gorham JM, et al. Glycogen storage diseases presenting as hypertrophic cardiomyopathy. N Engl J Med. 2005;352(4):362–72.
73. Bayrak F, Komurcu-Bayrak E, Mutlu B, Kahveci G, Basaran Y, Erginel-Unaltuna N. Ventricular preexcitation and cardiac hypertrophy mimicking hypertrophic cardiomyopathy in a Turkish family with a novel PRKAG2 mutation. Eur J Heart Fail. 2006;8(7):712–5.
74. Engberding R, Bender F. Echocardiographic detection of persistent myocardial sinusoids. Z Kardiol. 1984;73(12):786–8.
75. Stöllberger C, Finsterer J. Left ventricular hypertrabeculation/noncompaction. J Am Soc Echocardiogr. 2004;17(1):91–100.
76. Hofer M, Stöllberger C, Finsterer J. Acquired noncompaction associated with myopathy. Int J Cardiol. 2007;121(3):296–7.
77. Ichida F. Left ventricular noncompaction. Circ J. 2009;73(1):19–26.
78. Zaragoza MV, Arbustini E, Narula J. Noncompaction of the left ventricle: primary cardiomyopathy with an elusive genetic etiology. Curr Opin Pediatr. 2007;19(6):619–27.
79. Biagini E, Ragni L, Ferlito M, et al. Different types of cardiomyopathy associated with isolated ventricular noncompaction. Am J Cardiol. 2006;98(6):821–4.
80. Oechslin EN, Attenhofer Jost CH, Rojas JR, Kaufmann PA, Jenni R. Long-term follow-up of 34 adults with isolated left ventricular noncompaction: a distinct cardiomyopathy with poor prognosis. J Am Coll Cardiol. 2000;36(2):493–500.
81. Aras D, Tufekcioglu O, Ergun K, et al. Clinical features of isolated ventricular noncompaction in adults long-term clinical course, echocardiographic properties, and predictors of left ventricular failure. J Card Fail. 2006;12(9):726–33.
82. Xing Y, Ichida F, Matsuoka T, et al. Genetic analysis in patients with left ventricular noncompaction and evidence for genetic heterogeneity. Mol Genet Metab. 2006;88(1):71–7.
83. Hershberger RE, Lindenfeld J, Mestroni L, Seidman CE, Taylor MRG, Towbin JA. Genetic evaluation of cardiomyopathy–a Heart Failure Society of America practice guideline. J Card Fail. 2009;15(2):83–97.
84. Jenni R, Oechslin E, Schneider J, Attenhofer Jost C, Kaufmann PA. Echocardiographic and pathoanatomical characteristics of isolated left ventricular noncompaction: a step towards classification as a distinct cardiomyopathy. Heart. 2001;86(6):666–71.
85. Chin TK, Perloff JK, Williams RG, Jue K, Mohrmann R. Isolated noncompaction of left ventricular myocardium. A study of eight cases. Circulation. 1990;82(2): 507–13.
86. Belanger AR, Miller MA, Donthireddi UR, Najovits AJ, Goldman ME. New classification scheme of left ventricular noncompaction and correlation with ventricular performance. Am J Cardiol. 2008;102(1): 92–6.
87. Finsterer J, Stollberger C. Definite, probable, or possible left ventricular hypertrabeculation/noncompaction. Int J Cardiol. 2008;123(2):175–6.
88. Petersen SE, Selvanayagam JB, Wiesmann F, et al. Left ventricular non-compaction: insights from cardiovascular magnetic resonance imaging. J Am Coll Cardiol. 2005;46(1):101–5.
89. Lofiego C, Biagini E, Pasquale F, et al. Wide spectrum of presentation and variable outcomes of isolated left ventricular non-compaction. Heart. 2007;93(1):65–71.
90. Takano H, Komuro I. Beta-blockers have beneficial effects even on unclassified cardiomyopathy such as isolated ventricular noncompaction. Intern Med. 2002;41(8):601–2.
91. Epstein AE, Dimarco JP, Ellenbogen KA, et al. ACC/AHA/HRS 2008 Guidelines for device-based therapy of cardiac rhythm abnormalities. Heart Rhythm. 2008;5(6):e1–62.